



Spatial modelling of Cs-137 and Sr-90 fallout after the Fukushima Nuclear Power Plant accident

Sevim Bilici^{1,2} · Fatih Külahcı¹  · Ahmet Bilici^{1,3}

Received: 30 April 2019 / Published online: 19 August 2019
© Akadémiai Kiadó, Budapest, Hungary 2019

Abstract

Determination of radionuclides transport characteristics is among the most significant research topics, which require extensive multidisciplinary works. The spatial modeling methods are suggested to determine the effects of radioactive fallout. The spatial analysis has a history of approximately 250 years based on micro-scales, but today it has extended to macroscopic systems. After Fukushima accident, radioactive fallout in water and bottom sediment samples are collected from the deepest tectonic freshwater lake in Turkey, Hazar Lake, and Point Cumulative SemiVariogram and Triple Diagram models are employed for depiction their features.

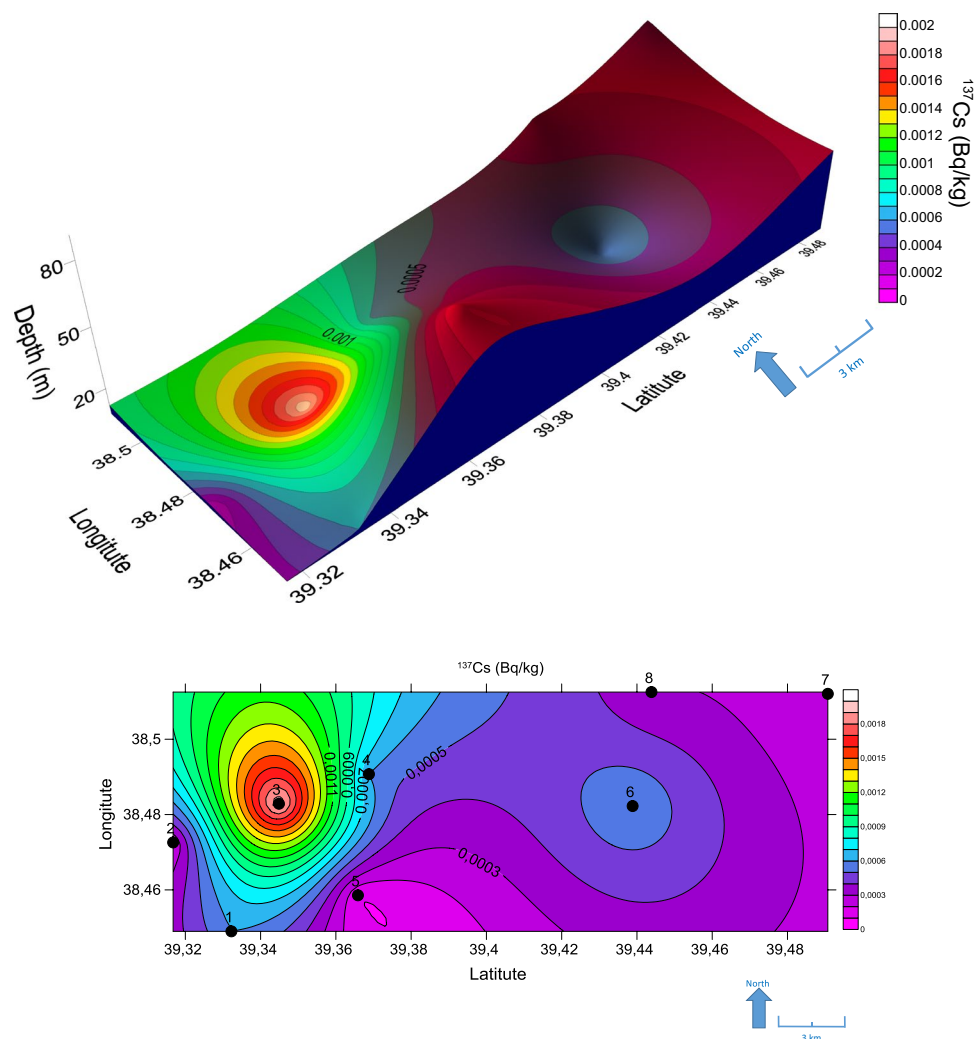
✉ Fatih Külahcı
fatihkulahci@firat.edu.tr

¹ Nuclear Physics Division, Department of Physics, Faculty of Science, Firat University, 23119 Elazig, Turkey

² Department of Opticianry, Vocational School of Health Service, Bandirma Onyedi Eylul University, Bandirma, Turkey

³ Department of Medical Imaging Techniques, Vocational School of Health Service, Bandirma Onyedi Eylul University, Bandirma, Turkey

Graphic abstract



Keywords Geostatistical modelling · Radionuclide transport · Weighting methods · Radioactive fallout · Simulation

Introduction

The energy requirement for human activities is in increase, and hence it is necessary to increase the diversity of the energy acquisition types and efficiencies. Nuclear energy is one of the best sources of enormous energy supply with very little fuel and greenhouse gas emissions. The standards adopted by the International Atomic Energy Agency must be applied strictly for their operation; otherwise, accidents may cause to global disasters [1]. Nuclear power generation through nuclear power plants continues unabated manner, even though some accidents have occurred, among which are Three Mile Island (1979), Chernobyl (1986) and Fukushima (2011) nuclear accidents [2]. Experts of Fukushima Dai-Ichi Nuclear Power Plant

Accident (FDNPPA) describe it as the largest nuclear accident after Chernobyl Nuclear Power Plant Accident, where the reactor had user error and caused a tremendous release of radioactivity to the environment [3–13]. Radionuclides can be transported thousands of miles away due to atmospheric events [14–19]. In the FDNPPA, the reactor cooling system was damaged by 9 magnitude earthquake and subsequent tsunami, and hence, the reactor melted partially [20]. After FDNPPA, radioactive fission products between the Fukushima Dai-Ichi Nuclear Power Plant (FDNPP) and neighbouring provinces have spread widely and led to serious soil pollution with regional as well as global radionuclides dispersions. Fission products from the accident spread not only in the entire northern hemisphere, but also in the southern hemisphere [21–27].

The most important biological effects of radionuclides from such accidents are due to the environment long half-lives of ^{137}Cs (30.1 years) and ^{90}Sr (29 years) isotopes. Their artificial radionuclides activities are important research topics in the air, soil and water [28–37]. The radionuclides concentrations determination is very important as for the living organisms' health is concerned. One of the most significant steps is to evaluate the radionuclides concentrations in the region by means of a convenient model [38–58]. Once the validity of such a model is established then it is possible to obtain appropriate information as for the transport amount of the activity concentrations in different radionuclides [59, 60]. In order to provide all these facilities, after the Chernobyl and Fukushima nuclear reactor accidents, various authors proposed different models and methods to analyse spatially the radioactive fallout clouds migration [2, 61–71].

Spatial [72, 73] and spatio-temporal models [74–76] have significant advantages in depicting the radionuclides effects on atmosphere [7] and surface transports [77–79]. It is possible to conclude that many researches have applied such spatial models from micro- [80–82] to macro-scales [82, 83]. The first examples of the spatial modeling is due to Halley [84], who showed the directions of monsoons and winds on equally divided maps, and concluded about the physical cause of these wind formation. Student [85], performed spatial modeling by dividing 1 mm^2 into 400 equal parts to count the yeast cells. According to cell number in the unit area the probability distribution functions (PDFs) has been obtained, which is regarded as the first spatial modeling study by many researchers. Spatial modeling is useful to determine the spatial distribution of geomagnetic fluctuations [86] in the determination of mineral metaformic rocks paragenesis [87], in seismic estimation studies [88], in the seismic body waves propagation determination [89], in hydrology [90], and in electromagnetic interactions studies [91], in the determination of ^{235}U concentrations in marine sediments [92], in the climate changes clarification [93], and in the geophysical studies [74, 94–98].

The Point Cumulative Semivariogram (PCSV) technique is employed for spatial modelling and its calculations are based on mathematical principles. Its validity depends on the classical variance and covariance techniques for regular distribution in the spatial analyses that comply with the normal PDF. In practical works, the measurement locations are frequently irregularly spaced. Matheron [99] suggested a semi-variogram (SV) technique, which is a very useful metric that expresses the difference square between the regional variable (ReV) measurements depending on the distance. Later, Şen [100] proposed the Point Cumulative Semi-Variogram (PCSV) method, which has all the features of the classical SV, and at the same time, it further enhances the properties of classical SV. The PCSV method is used when the sampling points are scattered irregularly [97, 101–103].

In this study, after the occurrence of FDNPPA, PCSV [100] and TDM [104–106] methods are proposed to investigate transport characteristics, and the effects of ^{137}Cs and ^{90}Sr radionuclides radioactive fallout for Hazar Lake, Turkey. In this study the depth parameter is also considered. This latter method is preferred, because it has significant advantages for the transport and radioactive fallout characterization. The water depth is important to see the consequences of the global transport of the relevant radionuclides, and besides, it is important in the radionuclides concentrations amount [107]. For this reason, the lake depth is also included in the modelling process, so that a three-dimensional spatial analysis is suggested for the radioactive particles. Furthermore, re-assessments are made on spatial modeling and atmospheric radioactivity transport. Finally, the iso-radioactivity diagrams are drawn and interpreted for ^{137}C and ^{90}Sr radioactive fallout products.

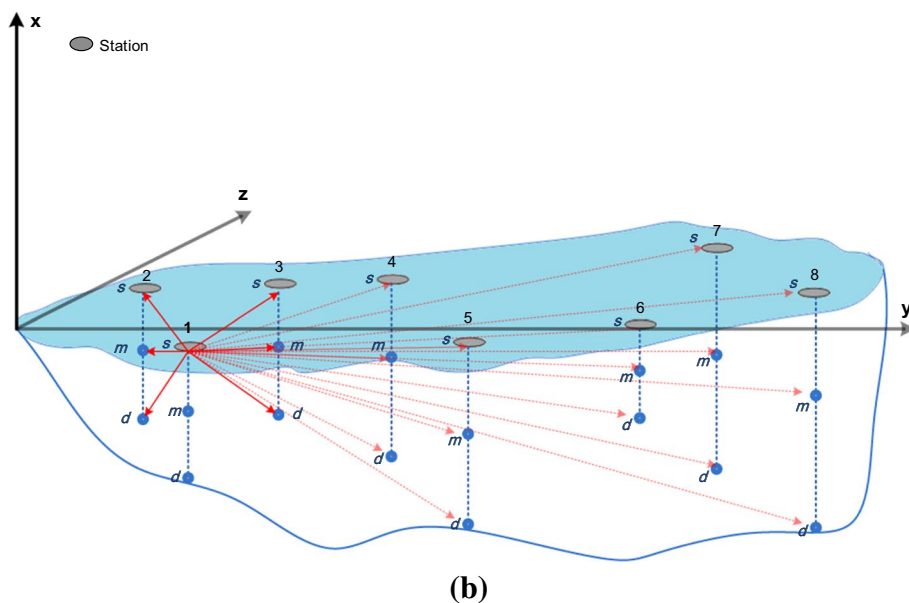
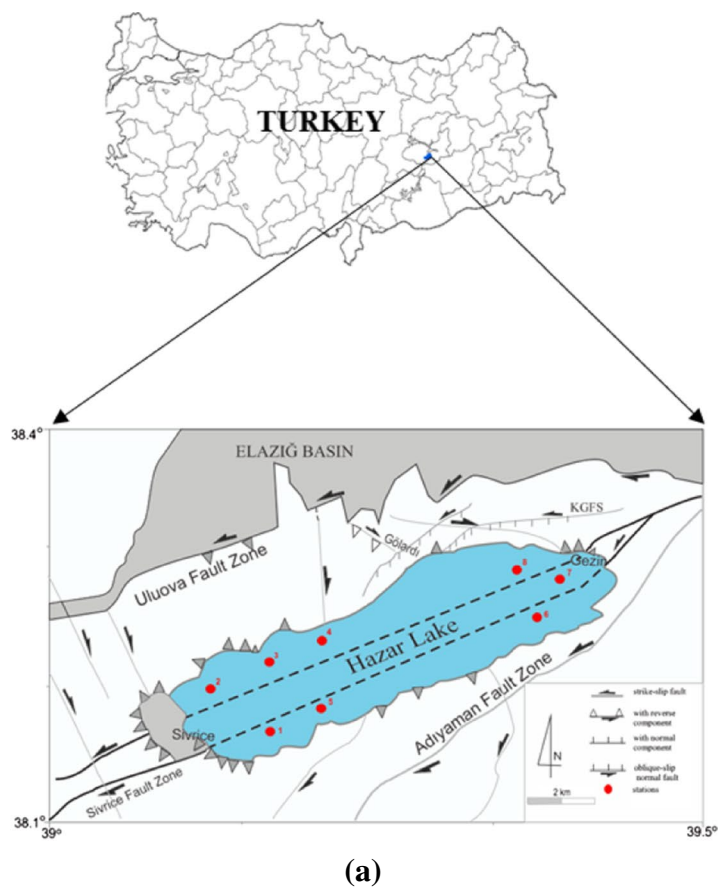
Research area and experimental studies

The Hazar Lake and sampling selected stations in the research area are given in Fig. 1. The lake is one of the deepest (250 m) freshwater in the world [108, 109]. It extends in the northeast-southwest direction along the Eastern Anatolian Fault at an altitude of 1255 m and its width is 7 km with 25 km length [110, 111]. One of its interesting features is a tectonic feature directly above the Eastern Anatolian Fault Zone (EAFZ), which is a seismically active strike-slip left-hand fault zone in this part of the world [112]. The southern coastline of the lake is very flat and fault-controlled and limited by the rise of the Caspian Mountain (2350 m). The northern coastline is not associated with any faulting [110]. At places, where the active fault lines are known, higher environment natural radioactivity is identified than other regions [97].

Basin sediments mainly originate from two main drainage systems confluence with the lake at the south-western and north-eastern ends. The Kürkçayı River forms an important alluvial fan in the southwest drainage system, and it is the largest drainage system. The Northeast drainage system consists of several streams with small drainage areas. The main rock in the collection area consists mainly of magmatic, metamorphic and ophiolitic rocks of the Mesozoic and Palaeozoic periods. The mountainous area to the south of the lake consists of late Jurassic magmatic rocks and middle Eocene limestones [110, 111].

Water and bottom sediment sample stations constitute the material of this study and such a research has attracted the attention of many researchers in the past due to the morphological, geological and tectonic features as given in Fig. 1. A total of 24 water samples are taken from different depths

Fig. 1 **a** Hazar Lake and sampling stations. **b** 3D representation of the Hazar Lake sampling points. Each of the 8 stations created for sampling is divided into three groups as surface (*s*), middle (*m*) and deep (*d*) depths. **b** Shows the measurement of the distances from the reference station (number 1) to the other stations for PCSV modeling. After this measurement, the distances from station 2 to other stations are measured by passing to station 2, which is done for all groups (*s*, *m*, *d*) of all other stations (see “Point cumulative semivariogram modelling” section for theoretical explanations)



(surface, medium and bottom) at each station in addition to 8 bottom sediment samples for determination the activity concentrations of ^{137}Cs and ^{90}Sr radionuclides.

Determination of ^{137}Cs and ^{90}Sr activity of water samples and bottom sediment samples

To pick up the water samples, a Nansen tube and a dipper are used to get the bottom sediment. Sterilized 1 L glass

bottles are used for radioactivity analysis of water samples. Three samples are taken from the same bottle with the help of 100 mL beakers cleaned with pure water. After evaporating the water samples with the help of the heater (60 °C), the remains are taken by spatulas and placed in aluminium tables with a surface area of 11.34 cm² and a depth of about 4–5 mm with pure water. After drying the sediment in the liquid phase in the trays, the activity concentration counts are performed with the gamma/beta sensor counting system (ST7 scintillation counter) to perform gamma/beta radioactivity analyses of the samples. A well-type gamma-spectrometric system with 2" × 2" NaI (TI) detector was used for the analysis of the radionuclides. The system has a 3.5 cm thick cylindrical lead shield that prevents external radiation. ⁶⁰Co (1 μCi) and ²²⁶Ra (10 μCi) spot sources were used for energy calibration of the detector system.

To improve statistical confidence for each sample, the measurements are repeated 3 times and then the arithmetic mean is considered as representative. The following expression provides the activity concentrations are calculated for each sample.

$$A = \frac{C}{\varepsilon \cdot P \cdot V_s} \text{ Bq/L} \quad (1)$$

where C is the unit time count, ε is the detector efficiency, P is the probability for the characteristic gamma/beta rays, V_s is the volume of the sample, and A is gamma/beta activity in terms of Bq. The activity concentrations of ⁹⁰Sr and ¹³⁷Cs are evaluated using its 546 keV peak and 661.6 keV peak, respectively [113].

One of the aims is to carry out radioactivity analyses of the bottom sediment samples for possible change and transport of ¹³⁷Cs and ⁹⁰Sr in the bottom sediment. The extraction of the bottom sediment samples is done together with the water sampling procedure. After similar procedures in the water samples, the sediment samples are weighed by transferring to the tared planchets and thus a sediment amount is calculated for each sample. Sediment samples are collected using a stainless steel dipper. Sediment samples are put into polyethylene bags and stored at 4 °C and transported to the laboratory. The sediments are dried in an oven at 50 °C for 48 h. All samples are counted by the gamma/beta sensor counting system for activity determination. The following expression is used for the activity concentrations of the samples [113].

$$A = \frac{C}{\varepsilon \cdot P \cdot M_s} \text{ Bq/kg} \quad (2)$$

where V_s in Eq. (1) is replaced M_s , which is the quantity of the sample.

The standard deviation of the measurements has changed between 5 and 10%. The internal quality control

is checked using certified reference material, IAEA-384, within ± 1 standard deviation (SD) of the reference value. The accuracy and precision of radiochemical determination of ¹³⁷Cs and ⁹⁰Sr are approximately 5% [114].

Theoretical studies for radioactive fallout

Point cumulative semivariogram method

Variance and correlation techniques are frequently used in the literature to measure the degree of regional dependence in spatial variables. These methods cannot fully express regional dependence due to the non-normal PDFs or the irregularity of the sample locations [115].

The classic SV can make reliable estimates for small distances when the distribution of sample points is regular within the region. As the distance increases, the number of data pairs decreases for the calculation of SV, which means less reliable estimation at larger distances [116]. The SV calculation process is similar to the time series analysis, and it helps to determine influence of distance, which specifies the area of dependence between uniformly distributed special points [117].

Şen [115], has proposed the Point Cumulative Semi-Variogram (PCSV) method, which is based on the relationship between the point and the area according to the absence of stationarity, and the irregular or random measurement sites distribution [118]. The PCSV method accounts for the regional effects of other sites within the study area, and the number of PCSVs is equal to the number of sites [119]. The PCSV can be defined as the sum of the half of the difference squared ranked according to distance values from smallest to the biggest distance. This method yields a non-decreasing experimental PCSV function for the site considered. The mathematical expression is given by Şen [100] as follows.

$$\gamma(d_i) = \frac{1}{2} \sum_{i=1}^{n-1} (Z_c - Z_i)^2 \quad (3)$$

where $\gamma(d_i)$ is the PCSV value at distance, d_i , of the corresponding station; Z_c is the regional variable value at the reference point, and Z_i ($i = 1, 2, \dots, n - 1$) is the value of the regional variable at other sites. The implementation steps of the PCSV method can be summarized as follows:

1. The reference site is selected, let us say site c , the distances between this and the other sites ($i = 1, 2, \dots, n - 1$) are calculated. If there are n sites, $n - 1$ is the number of distances.
2. For each pair, there are half-square differences between two data values. In this way, each distance has its own

half-square value as $\frac{1}{2}(Z_c - Z_i)^2$, where Z_c and Z_i are the regional variable values in the corresponding region and in i -site, respectively.

3. The distances are sorted from smallest to the largest and the sums of consecutive half-square differences are calculated for each distance. This method gives a non-decreasing experimental PCSV function at the site according to Eq. (3).
4. For other sites, sample PCSVs are calculated in the similar way by repetition of the previous steps.
5. A theoretical PCSV curve is fitted to the experimental PCSV scatter diagram by means of MATLAB® software program.

Triple diagram method

Triple diagram method is based on the fact that three regional variables are shown on a single diagram using the Kriging methodologies [120–123]. The corresponding change can be seen in detail and useful way than the classical Cartesian coordinate system. The triple diagram method is used for iso-radionuclide map constructions from all the numerical results.

Results and discussion

There are many factors that affect the behaviour and propagation of radionuclides after a nuclear accident [124, 125]. Much of the radioactive particle propagation depends on environmental conditions and events [126]. Factors such as wind direction, precipitation, moisture, soil structure, vegetation cover, soil pH value affect the propagation of these nuclides [127]. The radioactive particles transported to far distances along the winds are stored on the earth surface [128] and then radiated into the ground by radioactive precipitation [129, 130], causing radioactive contamination [131]. Precipitation and flooding erode the land on which radionuclides are stored [128]. These dissolved radionuclides reach rivers [132] and ground waters [133]. Another factor that affects the radioactive substances is water transport, which has different characteristics such as solubility, transportability and precipitation of different radioactive grains. Due to the strong flow velocities of the surface waters, the clay minerals are easily transported with potassium, rubidium, cosmic ray and artificial radionuclides in suspended particles [134–137]. ^{137}Cs is a radionuclide that radiates to the environment in the event of a nuclear accident, carried along long distances by meteorological events, and able to survive for a long-time in the ground [138]. After a nuclear accident, as well as the ^{137}Cs that spread to the Earth's atmosphere, the ^{90}Sr goes down to

the earth with sprinkles or rain like ^{137}Cs [7, 20]. Along the tendency of radioactive isotopes to accumulate in soils, waters and rocks are closely related to the geological structure of the environment [139]. Many environmental factors such as precipitation regime, soil structure, vegetation cover and geology of each region are also effective in the process [140]. Depending on these differences, the radionuclides distributions rates vary. All the factors that are mentioned above affect the accumulation and distribution of ^{137}Cs and ^{90}Sr , and therefore, cause to the distribution of ^{137}Cs and ^{90}Sr depending on the distance between the sample stations.

Both experimental and theoretical works are carried out in Hazar Lake. The activity concentrations of radionuclides in analysed samples, water depths, locations and the gamma energies are used for calculations of these activity concentrations, which are given in Table 1.

In this table, the letters a , b , and c represent the surface, medium and bottom depth distances of the corresponding sampling station, respectively.

In addition to the lake waters, concentrations of ^{137}Cs and ^{90}Sr are also determined in the bottom sediment samples (Table 2). Thus, it is understood that the radionuclide migration in water and bottom sediment changes in samples are more informative. The radionuclide measurements in Tables 1 and 2 have a standard deviation of $\pm 10\%$.

Normal PDF is the most important and employed one in different research applications. As in classical statistic, the geostatistical analysis is also expected to conform to the normal PDF [141, 142]. The data may not be suitable for normal PDF, and therefore in this study, transformations are applied to fit the normal PDF. ^{90}Sr in water and ^{137}Cs and ^{90}Sr activity concentrations in the bottom sediment abide with the normal PDF after logarithmic transformation. ^{137}Cs activity concentrations in water accord with normal PDF without logarithmic transformation. Normal PDF tests, Q–Q plot method and Shapiro–Wilk normality test are performed to see if the data are normally distributed. The Shapiro–Wilk test is the most powerful in comparing the forces of normality tests [143]. Figure 2 shows the normal PDF graphs of the ^{137}Cs and ^{90}Sr activity concentrations in the water and the relation between the expected and observed values. Similarly, Fig. 3 indicates the normal PDF graphs of the ^{137}Cs and ^{90}Sr activity concentrations in the bottom sludge. In addition, Pearson's r values are calculated to see the relationship between variables. Table 3 includes the results from the statistical analysis.

Depths are taken into consideration as important factors in determining the radionuclide activity concentration. The activity concentrations variation according to bottom sediment samples and the surface, middle and bottom depths of water sampling points from different parts of the lake are plotted for respective radionuclides in Fig. 4a–d.

Table 1 Sampling location coordinates and activity concentrations of water samples collected at Hazar Lake

Station number	Latitude (north)	Longitude (east)	Station details	Depth (m)	^{137}Cs (Bq/L) (661.6 keV)	^{90}Sr (Bq/L) (546 keV)
1	38,448	39,332	1a	0.15	0.705	0.451
			1b	4	1.032	0.542
			1c	8	0.872	0.662
2	38,472	39,316	2a	0.15	0.803	0.451
			2b	4	0.774	0.480
			2c	8	0.516	0.840
3	38,482	39,344	3a	0.15	0.479	0.961
			3b	5.5	0.631	0.331
			3c	11	0.946	0.660
4	38,490	39,368	4a	0.15	0.654	0.930
			4b	12	0.639	0.631
			4c	24	0.602	0.585
5	38,458	39,365	5a	0.15	0.896	0.435
			5b	32	0.533	0.391
			5c	64	0.413	0.731
6	38,482	39,438	6a	0.15	0.912	0.750
			6b	3	0.396	0.811
			6c	6	0.586	0.451
7	38,512	39,490	7a	0.15	0.447	0.860
			7b	45	0.516	0.495
			7c	90	0.551	0.494
8	38,512	39,443	8a	0.15	0.964	0.421
			8b	30	0.511	1.275
			8c	60	0.696	0.885

Table 2 Depths and activity values of bottom sediment stations

Stations	Depth (m)	^{137}Cs (mBq/kg)	^{90}Sr (mBq/kg)
1	9	0.6	0.1
2	9	0.2	0.2
3	12	2	3
4	25	0.6	0.7
5	65	0.1	0.1
6	7	0.6	0.6
7	91	0.2	0.4
8	61	0.3	0.1

Figure 4a, b and Table 1 present the maximum activity concentrations for the surface, middle and bottom distances of the ^{137}Cs and ^{90}Sr isotopes in the water samples. These values are 0.964, 1.032, 0.946 Bq/L for ^{137}Cs and 0.961, 1.275 and 0.885 Bq/L for ^{90}Sr , respectively. Mean activity concentrations of ^{137}Cs and ^{90}Sr are calculated as 0.7325, 0.629, 0.651 Bq/L and 0.657, 0.619 and 0.663 Bq/L for the surface, middle and bottom depths, respectively.

The results for activity concentration in water and sediment in different parts of the world are given in Table 4 for comparison purpose with the values measured in this

study, Fukushima Dai-Ichi nuclear power plant accident with no significant radioactivity Fukushima transfer to Turkey. Although this indicates that the result is negative, but this study shows the boundaries of the FDNPP effect, and this context provides an answer regarding the impact on Turkey. The accident offers an important result, because it serves the public interest.

Point cumulative semivariogram modelling

The distance-dependent changes in the regional variables in the study area (^{137}Cs and ^{90}Sr in this study) can be defined by the SV functions. The difference between the values of the regional variable at different sites is a function of the distance between these variables [156]. Since the PCSV method takes into account the effect of all the stations in any region, unlike the classical SV, the number of the PCSV graphs is equal to the number of stations. There are 24 different water-sampling sites, and therefore, 24 PCSV graphs (48 graphs in total) for ^{137}Cs and ^{90}Sr . Since there are eight positions for the bottom sediment samples, eight PCSV graphs (16 graphs in total) appear for each of the radionuclides. The least squares model fits theoretical curves to the scatter of PCSV values. The graphs show similar characteristics, and

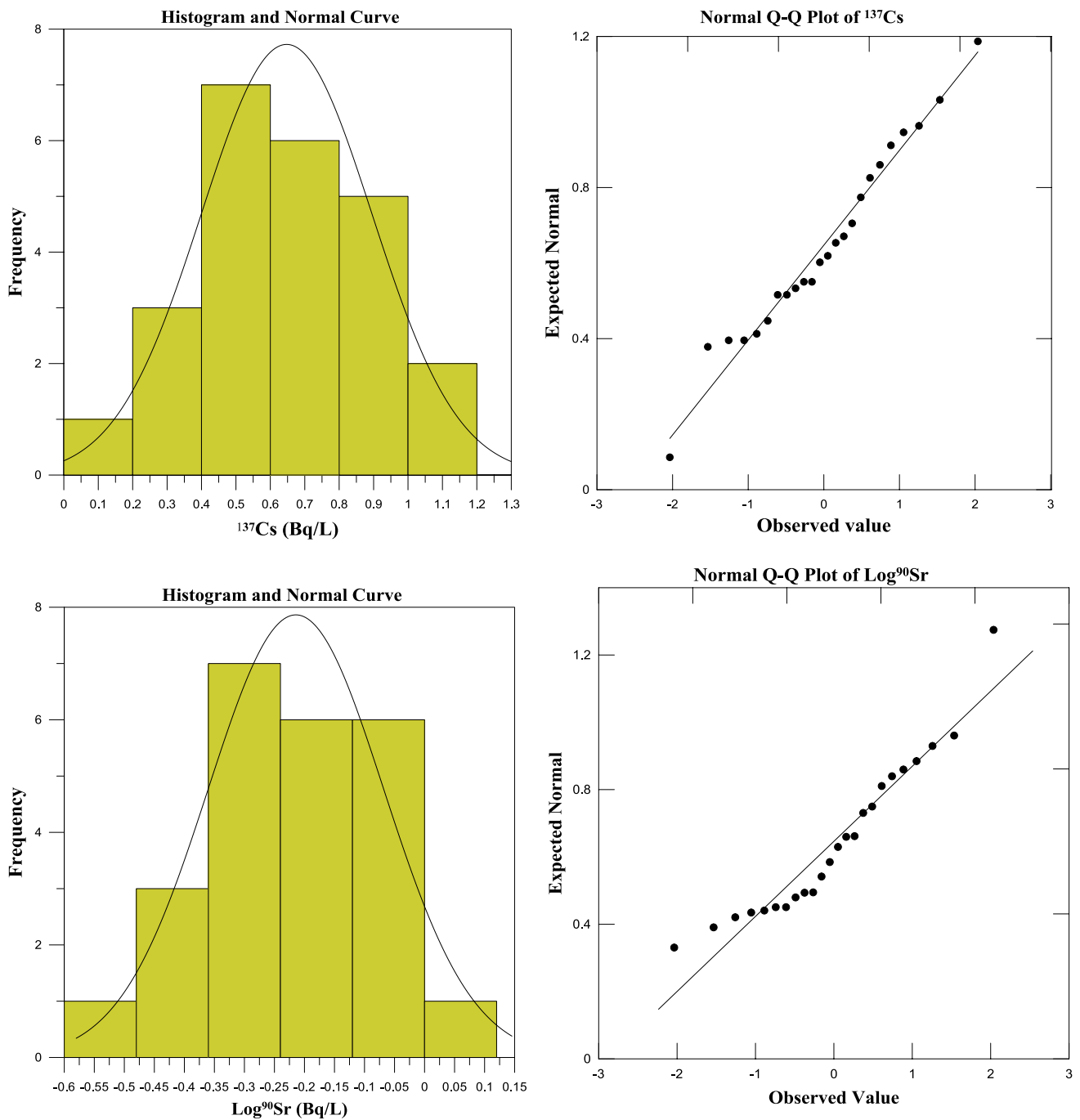


Fig. 2 Frequency distribution and Q–Q plots of the ^{137}Cs and ^{90}Sr activity concentrations in the water

therefore, they are grouped as in Fig. 5. The stations with the same fit curves are given as the PCSV models in Fig. 5 and Table 5.

A sample graph for the theoretical PCSV and the representation of its parameters are given in Fig. 6a. Figure 6b shows the original program output, which is the graph of the ^{137}Cs of 1c station in water. In this figure, the PCSV model curve remained almost constant after 13.11 km

(range). The stationary point of PCSV is defined as “Sill” in the geostatistical literature. On the other hand, the 1c ^{90}Sr PCSV graph also follows Model A (Table 5) with the range (1c, ^{90}Sr) about 13 km.

The model-matching stations in Fig. 6b are grouped as Model A (Table 5), and the same processes are performed for each of the other 63 stations with records in Table 5

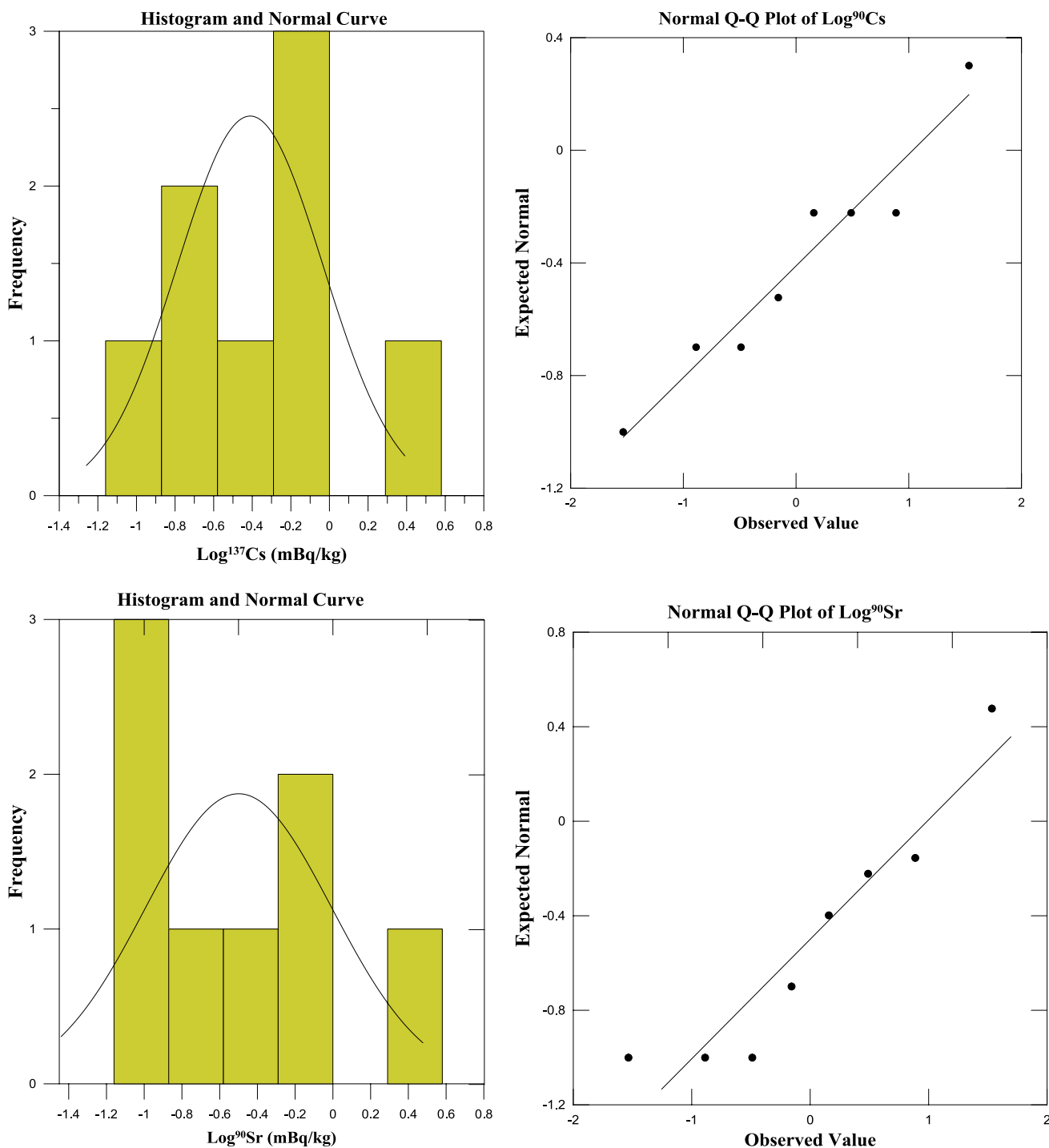


Fig. 3 Frequency distribution and Q–Q plots of the ¹³⁷Cs and ⁹⁰Sr activity concentrations in the bottom sediment

models in Fig. 5, where the theoretical PCSV graphs of the two radionuclides provide the following information.

If the distance between the sampling points increases, the variogram value also increases, and rises to an approximate constant value at a certain separation distance, which is referred to as the range. The appearance of the sill value in

the PCSV graphs can be explained as the weak contribution from other remote stations. The PCSV graphs of ¹³⁷Cs and ⁹⁰Sr 1c stations have the sill value for ¹³⁷Cs as 0.84, and for the ⁹⁰Sr as 1.769. It is obvious that the sill values are different for two variables although the same range value exists in the same region. The large sill value for these two variables

Table 3 Descriptive statistics for samples

Statistics	^{137}Cs (Bq/L)	^{90}Sr (Bq/L)	^{137}Cs (mBq/kg)	^{90}Sr (mBq/kg)
N	24	24	8	8
Mean	0.647	-0.214	-0.410	-0.499
SD	0.253	0.149	0.403	-0.527
Min.	0.090	0.480	-1.000	-1.000
Max.	1.190	0.110	0.300	-0.480
Skewness	0.151	-0.236	0.367	0.791
Kurtosis	0.018	0.754	0.209	0.041
Pearson's <i>r</i>	0.987	0.960	0.969	0.944
Shapiro–Wilk	0.838	0.851	0.678	0.212

Normality test $p > 0.05$

at the same distance indicates increase in the PCSV values, because the model curve approaches the PCSV axis. In this region ^{137}Cs and ^{90}Sr isotopes have the same range values, and the contribution of ^{137}Cs from the other stations is greater than ^{90}Sr . The distance up to the sill corresponds to the spatial dependence continues, which implies that the data are not related to one another along 13 km for the distribution of ^{137}Cs and ^{90}Sr around 1c station, and the distribution of ^{90}Sr in area 3c is about 16 km. Samples that are close to each other with a lower distance than the range value is spatially interrelated. The greater the effective distance, the greater is the influence of the variable. Samples that are separated from each other by a greater distance than the range value are not spatially related. Inspection of the graphs indicates that the range value of each graph is different from each other, which is due to the difference in distance from each station to another. The origin of the graph indicates that the regional dependency is zero at $h = 0$ (where h is the length over the y -axis of the nugget effect).

The stations defined in the Model B group are represented in Table 5 and Fig. 5. Logarithmic change means that the contribution from other stations to the station concerned is not homogeneous. According to SV methodology, as distance increases, the relationship between points decreases. In this context, when Model B is examined one can see that the variogram value does not increase as much as the initial value, and the increase in long distances decreases. In other words, with increasing distance, there is a decreasing contribution. Ideally, the SV should cross its origin as the distance between samples approaches zero. However, many activity values show non-zero SV values as h approaches zero.

The nugget effect in Model B reflects the difference between close samples, but not exactly in the same position, and it is usually due to measurement error or the nature of the examined variable [157, 158]. The nugget

effect varies in proportion to the increase in distance between the samples and the multiplicity of the data and finally it decreases with the compatibility of each other. If the nugget effect is large (small), the variance between the samples is high (low), and therefore, the variability is less.

Model C shows a change according to the Gaussian model and then goes on to a sudden increase. This model refers to phenomena that are similar in continuity or short distances [157, 159]. The variability is random after a different distance for each station on the x -axis, and the reason for this situation can be summarized for stations 1a and 1b match. After a certain distance from the surrounding stations (about 12 km), the contributions from other stations become more dominant, causing fluctuations in the concentration change. In addition, the presence of the nugget effect in the model indicates that these stations have their own characteristics. Indeed, there are only two stations that match Model B.

Model D shows a change according to Gaussian shape and has nugget effect. At stations 2a, 4c and 7b ^{137}Cs complies with this model and have a very small nugget effect of 0.02, which indicates less variability in the isotope, because it is scattered more intensely than other stations.

Model E shows an exponential change, which starts from an intersection point on the horizontal (distance) axis. This implies that the ^{90}Sr and ^{137}Cs isotopes exhibit the similar distribution for the respective stations at smaller distances than this intersection distance, so that there is a regional dependency. When the PCSV curves of the stations for Model E in Table 5 are examined, it is observed that the ^{90}Sr and the ^{137}Cs are homogeneously distributed for distances smaller than 0.4–1.3 km.

Stations in Model F exhibit a parabolic behaviour at the origin implying variable contribution from the other stations to the relevant station. Model G exhibits a convex curve and reaches the sill value with the PCSV charts matching the relevant stations with this model, which shows that the curve remained stable after an average of 8 km. This implies that these stations had no effect on each other after 8 km. This distance is 9 km for ^{137}Cs and approximately 7 km for ^{90}Sr . After this effective distance, the radionuclides do not have a spatial association. The impact distance of the ^{137}Cs relative to the ^{90}Sr means that the effect of ^{137}Cs continues at larger distances.

Model H is structurally similar to Model A but the only difference is in its nugget effect and similar interpretations can be made. Model I shows a logarithmic change unlike Model B, and it intersects the x -axis. Model J shows a logarithmic change and unlike Model B, but it does not have nugget effect, which indicates that the distributions of ^{90}Sr concentrations at stations 2c, 3a and 8a are homogeneous at nearby distances and heterogeneous at rather far sites.

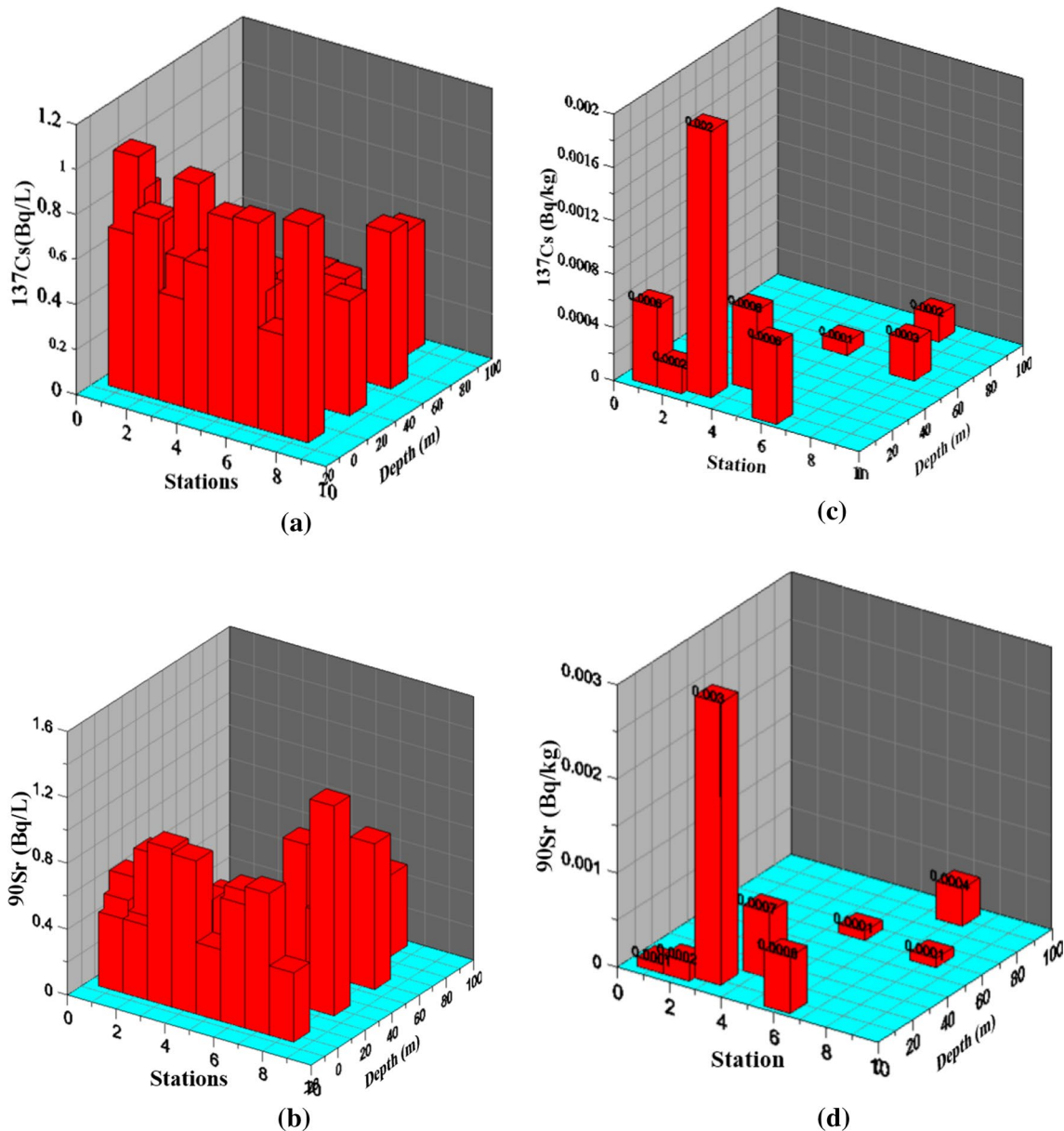


Fig. 4 **a** Change of ^{137}Cs activity for surface, middle and bottom water depths of the Hazar Lake, **b** change of ^{90}Sr in water samples, **c** change of ^{137}Cs in bottom sediment, **d** change of ^{90}Sr in bottom sediment

Modelling with triple diagram method

Iso-radioactivity maps are drawn in the sampling area by taking into account that ^{137}Cs and ^{90}Sr can be transported by flow in the water and bottom sediment media. These maps are the results of the triple diagram method, which shows the radionuclides transport characteristics at all depths in the lake. Figure 7 presents ^{137}Cs distributions, which are obtained in 3-dimensions for transport characterization at all depths in lake waters.

It is possible to see visually the distribution of the whole ^{137}Cs . Examination of the lake layers makes it partly possible to reach detailed interpretations in terms of depth. The triple diagram method is applied also for surface, medium, and deep depths for each radionuclide. The iso-radioactivity map for ^{137}Cs in surface waters is given in Fig. 8, where there is a high activity intensity in the north–south direction in the middle part of the lake (0.964–0.896 Bq/L), and also the ^{137}Cs mobility is high along this direction. As a consequence of the nuclear reactor accident, the ^{137}Cs spread

Table 4 Comparison of radioactivity concentration in this study with values reported for other locations in the world

Location	^{137}Cs		^{90}Sr		References
	(Bq/kg) ^a	(Bq/L) ^a	(Bq/kg) ^a	(Bq/L) ^a	
Turkey, Van Lake Basin	4.37	0.36	–	–	[144]
Turkey, Izmit Bay	21	–	–	–	[145]
Turkey, Black Sea Coast	0.56–5.43	–	–	–	[146]
Egypt, Nasser Lake	<0.01–19.7	–	–	–	[147]
Japan, Northern Basin	0.4–9.1	–	0.07–1.6	–	[148]
Japan, East Sea	0.0031 ± 0.0002	–	–	–	[149]
Korea	–	<4.00	–	–	[150]
Slovakia	–	–	3.4 ± 0.4	383.1 ± 45.3	[151]
Spain, Cádiz Bay	0.9–4.6	–	–	–	[152]
Chelyabinsk, Miass River	–	0.01–0.05	–	0.004–0.04	[153]
Ghana, Tano-North District	2.88 ± 0.12	–	–	–	[154]
Iran, Arvand River	1.96	–	–	–	[155]
Turkey, Hazar Lake	0.0001–0.002	0.396–1.032	0.0001–0.003	0.331–1.275	This work

^aMean or min–max

around the surrounding area, the radioactivity can be transported to distant places by meteorological phenomena and stay in the ground for a long time [160]. Almost 7–9% of the radionuclides in the soil containing ^{137}Cs pass to the water. In addition, meteorological factors play an important role in the distribution and behaviour of ^{137}Cs in different ecosystems [161, 162]. The bottom currents in the lake are quite strong and the lake has generally a wavy structure. These structural factors of the lake affect directly the transport of radionuclides.

In Fig. 9 ^{90}Sr exchanges are given in three-dimensional form in all lake depths. On the other hand, the surface waters ^{90}Sr iso-radioactivity map is shown in Fig. 10 from which it is possible to see that the activity value has high ^{90}Sr concentrations in the region surrounding the stations 3 and 4 (0.961–0.930 Bq/L). Furthermore, the activity intensity increases from the northern part to the coastal areas (0.860 Bq/L). According to other regions, the geology of the lake and the environment affect the distribution of the ^{90}Sr more and this nucleus cloud spreads to the atmosphere through the rain waters and accumulates more in the soil and rocks. In these areas, the coastal sector has a clayey structure, which can directly contribute to the radionuclides absorption.

Figure 11 is for the ^{137}Cs iso-radioactivity distribution in the middle depth waters, where the radioactivity values reach the highest value of 1.032 Bq/L in the southwestern part of the lake and the activity ratios increase in the coastal areas with intense magmatic formations that are remarkable on the north-west coast of the lake.

Figure 12 indicates that in the case of medium depth waters for ^{90}Sr the highest activity value (1.275 Bq/L) appears in the northern part of the lake. In the same way, it is observed that the activity towards shoreline increases in this region.

When the ^{137}Cs iso-radioactivity map at the bottom depths (Fig. 13) is examined, it is found that the highest value (0.946 Bq/L) is reached in the south-west part of the lake as in the middle depth waters. In addition, activity density is high in the western part of the lake (0.872 Bq/L).

In Fig. 14, at the bottom waters the highest activity of the ^{90}Sr is in the northern part of the lake (0.885 Bq/L), similar to the middle depths. ^{90}Sr is especially high around the eighth and second stations, which is about 40% of the coastal slope, which can be due to the large amount of soil, rock and similar deposits entering the lake. On the other hand, the eighth station is at the skirts of Hazar Baba Mountain, consists of metamorphic and volcanic rocks with completely natural radioactivity.

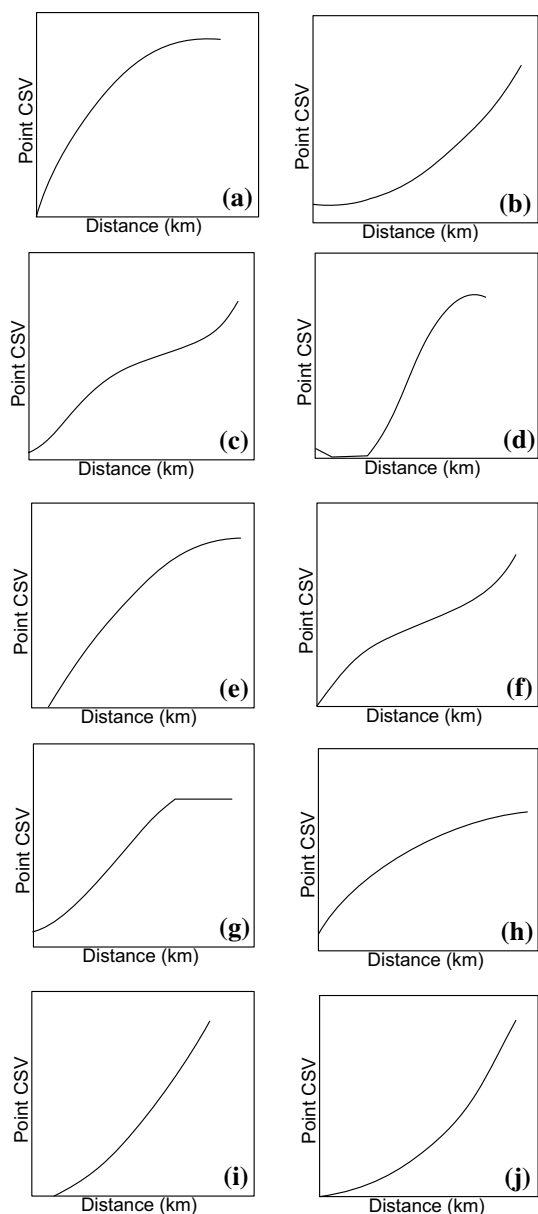


Fig. 5 PCSV models plotted for 64 graphs in overall total. Since the PCSV method obtained one graph representing each station, the model curves that characterize the stations are drawn. The stations are then grouped as in Table 3 and the results are interpreted

Artificial radioactivity in the bottom sediment is found to have equivalent radioactivity values with very small differences. One can conclude that these radio-cores show

a similar distribution in the sampling points. 2D and 3D graphics are drawn for the change in the bottom sediment of both radio-grains. The highest activity values are around Station 3. There is a continuous substance exchange between the lake and the surrounding coastal strip. Strong currents are observed in the bottom of the lake and on its surface, which entrain with various physical and chemical components. From the western coast of the lake, the Kürk River flows towards this station and 80,000 tons of clay-silt is pushed into the lake per year [108]. This factor is the most important effect when ^{137}Cs and ^{90}Sr values are high around this station (Figs. 15, 16).

One can see in Figs. 15 and 16 the coexistence conditions are similar at the two radionuclides.

Conclusions

In this study, ^{137}Cs and ^{90}Sr activity concentrations are analysed in water and bottom sediment samples that are collected in Hazar Lake, Turkey. The collected data are modelled by Point Cumulative Semi-Variogram (PCSV) technique, which is an advanced geostatistical method. On the other hand, three-dimensional spatial analysis is also performed for map constructions, the comparison between the measurement results and the case of Fukushima accident is achieved for the purpose to determine whether radioactive material transfer risk reached to Turkey. Two important results are obtained as the measurements confirmed such that the water and bottom sediment samples contain some radionuclides from Fukushima, they are below the world averages, and hence, the results do not constitute a health problem for the public radiologically. This study provides a basis for identifying the possible impacts of nuclear power plants on the environment and possible future changes observations. On the modelling side, the Triple Diagram Method (TDM) provides the distribution of rather large variables easily by considering the innovative geostatistical method as, the Point Cumulative Semivariogram (PCSV). These two methods provide great convenience in interpreting large scale environmental systems in terms of related regional variables. The variation in the transport, propagation, and quantities of the variables can be easily interpreted and visually observed for the study regions.

Table 5 Distribution of graphs drawn for ^{137}Cs and ^{90}Sr in water and bottom sediment samples of all stations according to PCSV models

PCSV models	^{137}Cs water stations	^{137}Cs bottom sediment stations	^{90}Sr water stations	^{90}Sr bottom sediment stations
A	1c		1c, 3c	
B	3b, 6a, 6c, 8a, 8c		3b, 5b, 5c, 6a, 8b, 8c	8
C	1a, 1b			
D	2a, 4c, 7b			
E	7a	1, 2, 3	1a, 2b, 5a, 6b, 7c	2, 3
F	3a, 4a, 5c, 6b, 8b		1b	
G	5a, 7c		2a	
H	2b, 3c, 4b	4, 5	4a, 4b, 4c, 6c, 7a, 7b	1, 4, 5
I	2c, 5b	6, 7, 8		6, 7
J			2c, 3a, 8a	

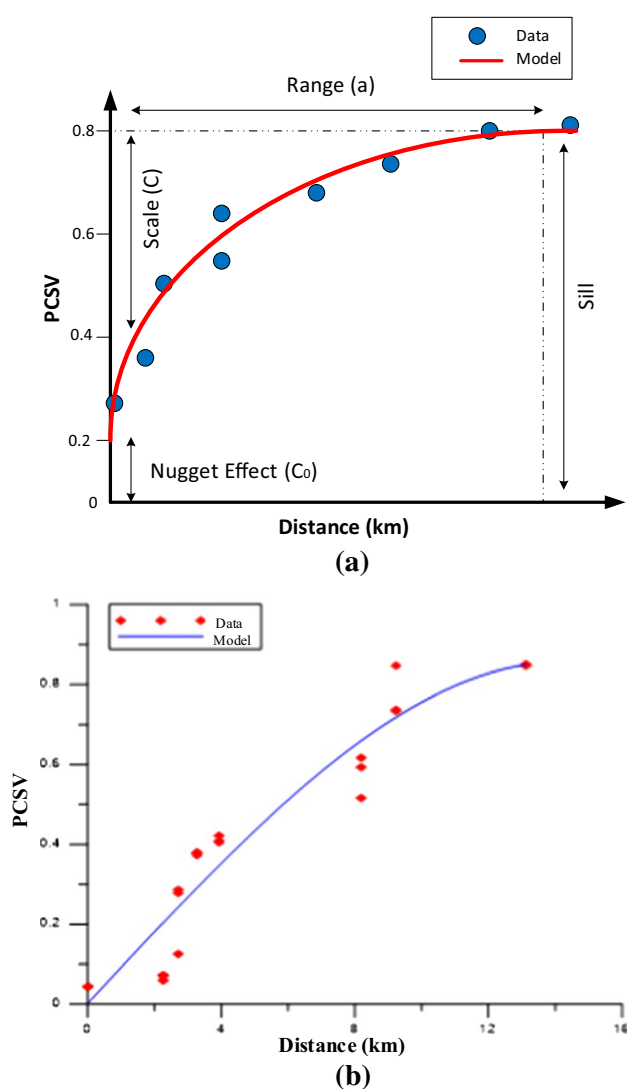


Fig. 6 a Theoretical PCSV graph and its parameters. b Experimental PCSV graph obtained for ^{137}Cs water 1c station. This graphic is selected as an example and the original program is output

Observed PCSVs for ^{137}Cs in water samples are calculated according to five and for ^{90}Sr to four different models. Concentrations of ^{137}Cs and ^{90}Sr from the same stations show very large distributional differences, and two artificial radionuclide have the mobility capacities that are weak in the bottom sediment samples with similar behaviours except for one of the PCSV graphs. It is possible to say that the contributions of the stations to each other and the environmental factors in the bottom sediment sampling sites are partly equal to the behaviour of these two radionuclides.

The PCSV and TDM methods gave important clues about the transport characteristics of the two radionuclides in the lake. These changes encourage one to monitor or characterize aforementioned methodologies for other radionuclides or harmful substances. The ^{137}Cs concentrations are low in the waters in the north western part of the lake and the main reason is the presence of external water inlets in these parts for low concentration. PCSV clearly shows the transport characteristics of the radionuclide. The transport characteristics of ^{90}Sr and ^{137}Cs in the bottom sediment appear to be very similar. These two radionuclides are deposited in the northwest part of the lake, which is supported by TDM graphs. The behaviour of ^{137}Cs and ^{90}Sr in water has a negative correlation and hence, it is possible to conclude that the presence of two radionuclides in one medium at the same time has a negative effect as one increases and the other decreases. This inverse correlation is also supported by the case TDM graphs.

Fig. 7 Three-dimensional change of ^{137}Cs in surface, middle and bottom waters of Hazar Lake

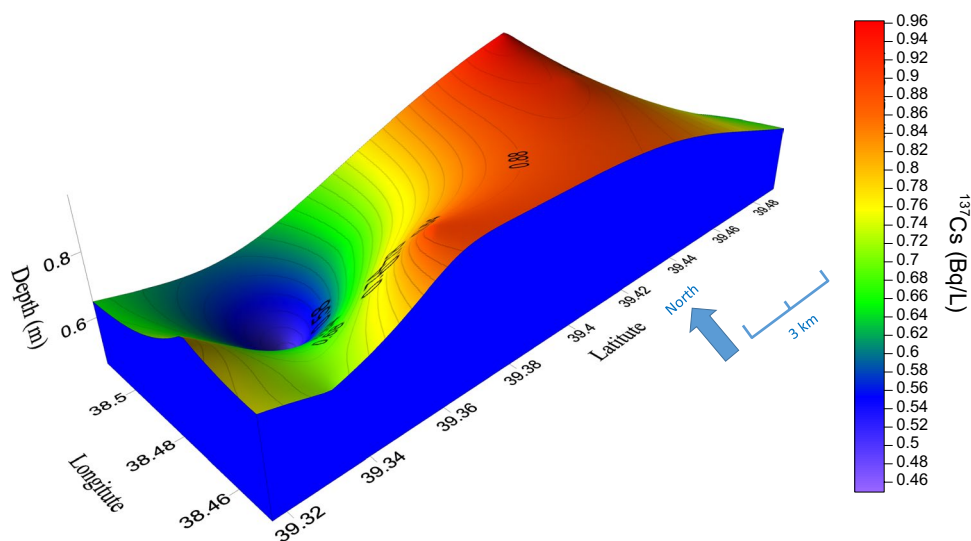


Fig. 8 Surface water ^{137}Cs iso-radioactivity map

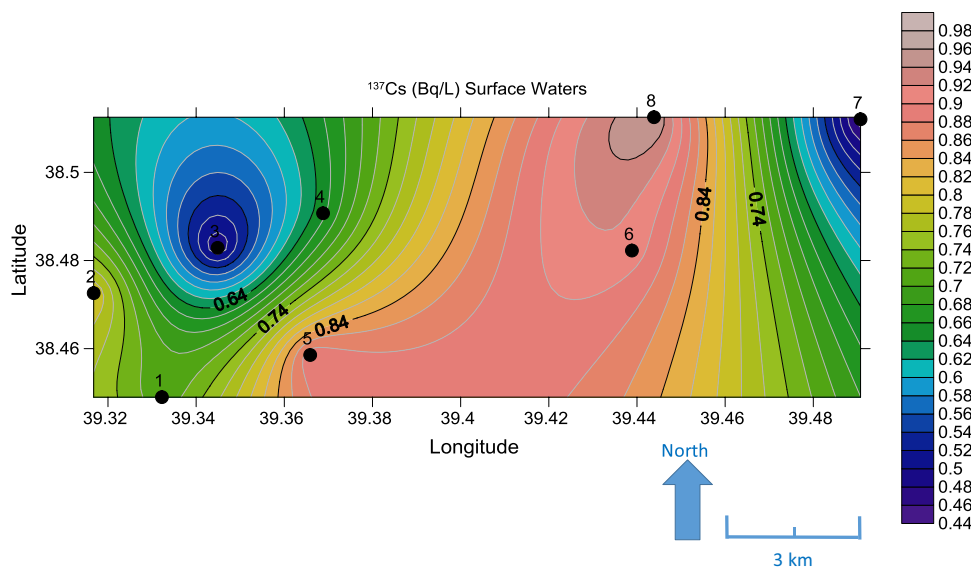


Fig. 9 Three-dimensional change of ^{90}Sr in surface, middle and bottom waters of Hazar Lake

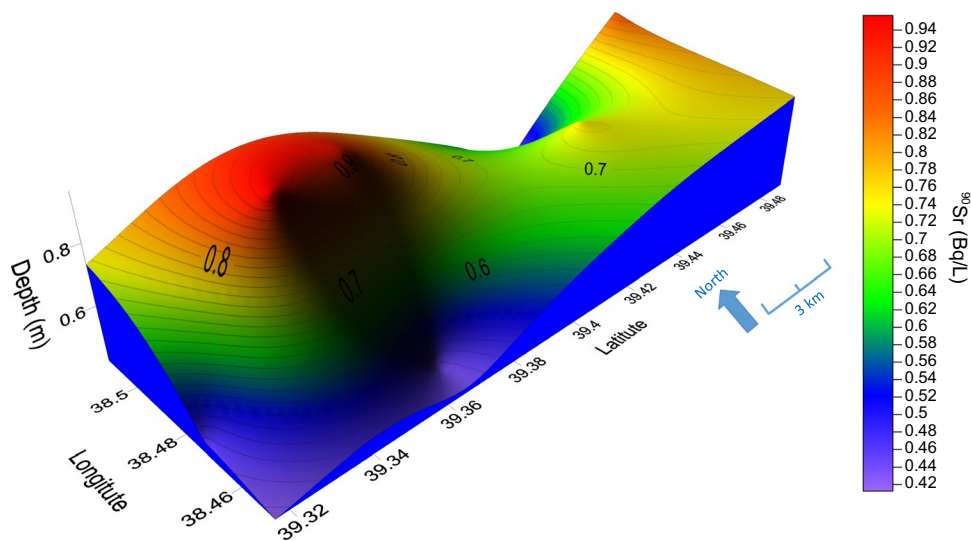


Fig. 10 Surface waters ^{90}Sr iso-radioactivity map

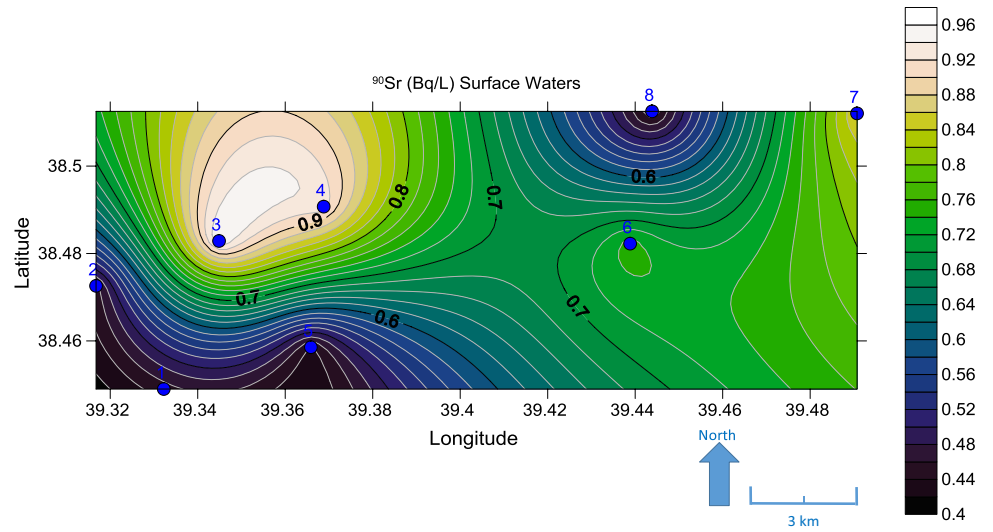


Fig. 11 Medium depth waters, ^{137}Cs iso-radioactivity map

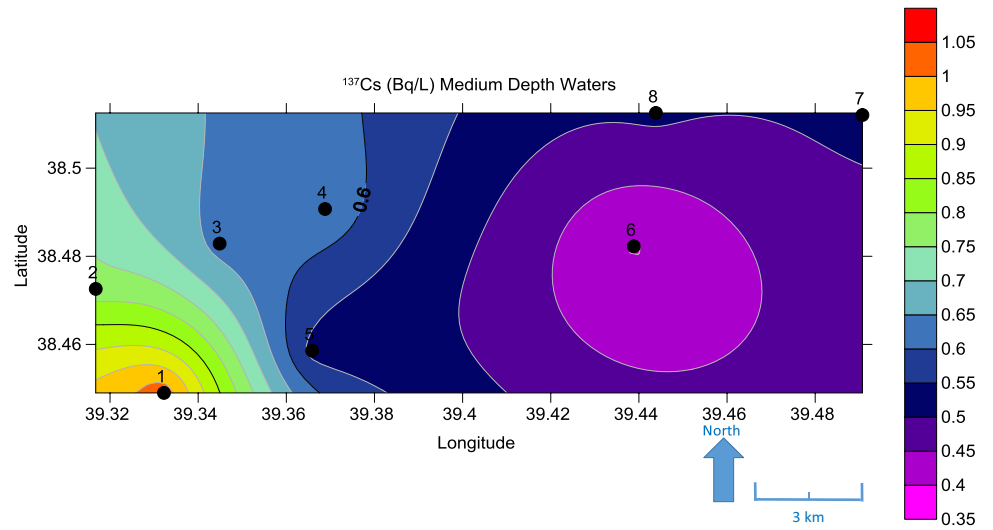


Fig. 12 Medium depth waters, ^{90}Sr iso-radioactivity map

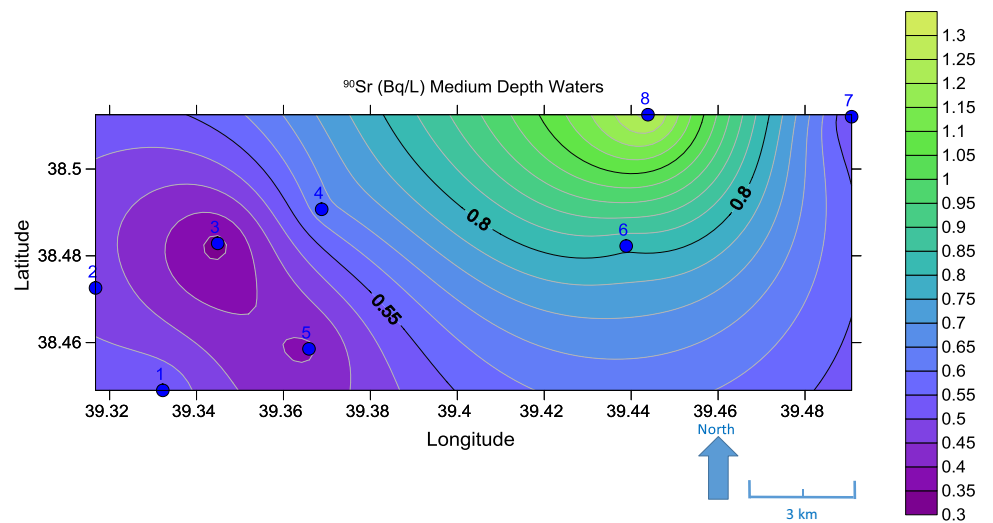


Fig. 13 Bottom depth waters, ^{137}Cs iso-radioactivity map

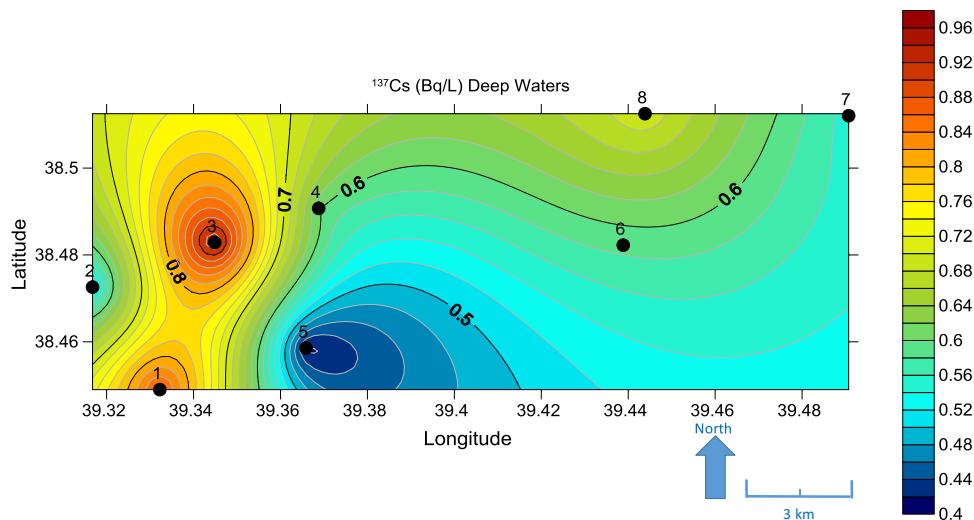
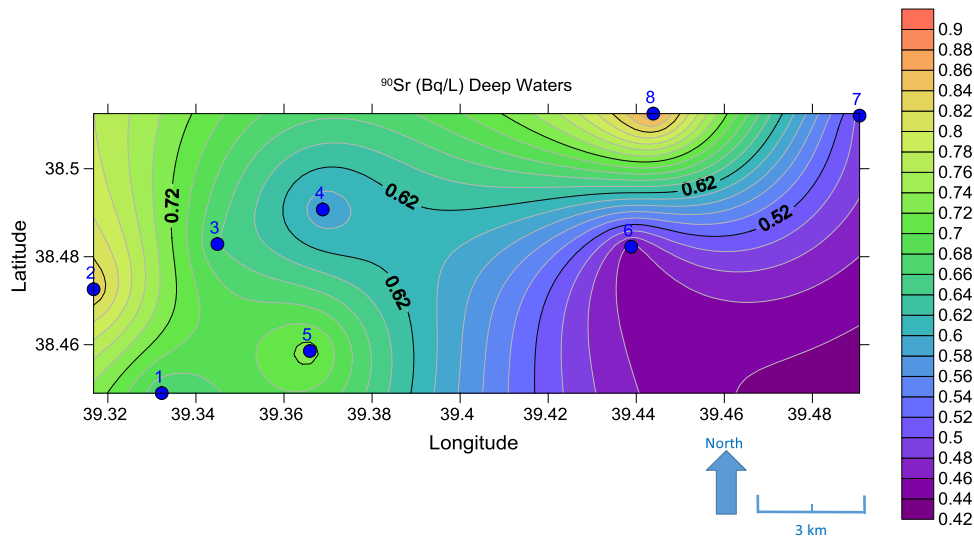


Fig. 14 Bottom depth waters, ^{90}Sr iso-radioactivity map



Finally, the lake has a tectonic structure and is in the middle of the elevations as a result of tectonic pit. The activity rates are relatively low compared to other parts of the world,

leaving the burden of radioactive fallout on these mountain and hills.

Fig. 15 ^{137}Cs **a** three-dimensional and **b** two-dimensional iso-radioactivity diagrams in the bottom sediment

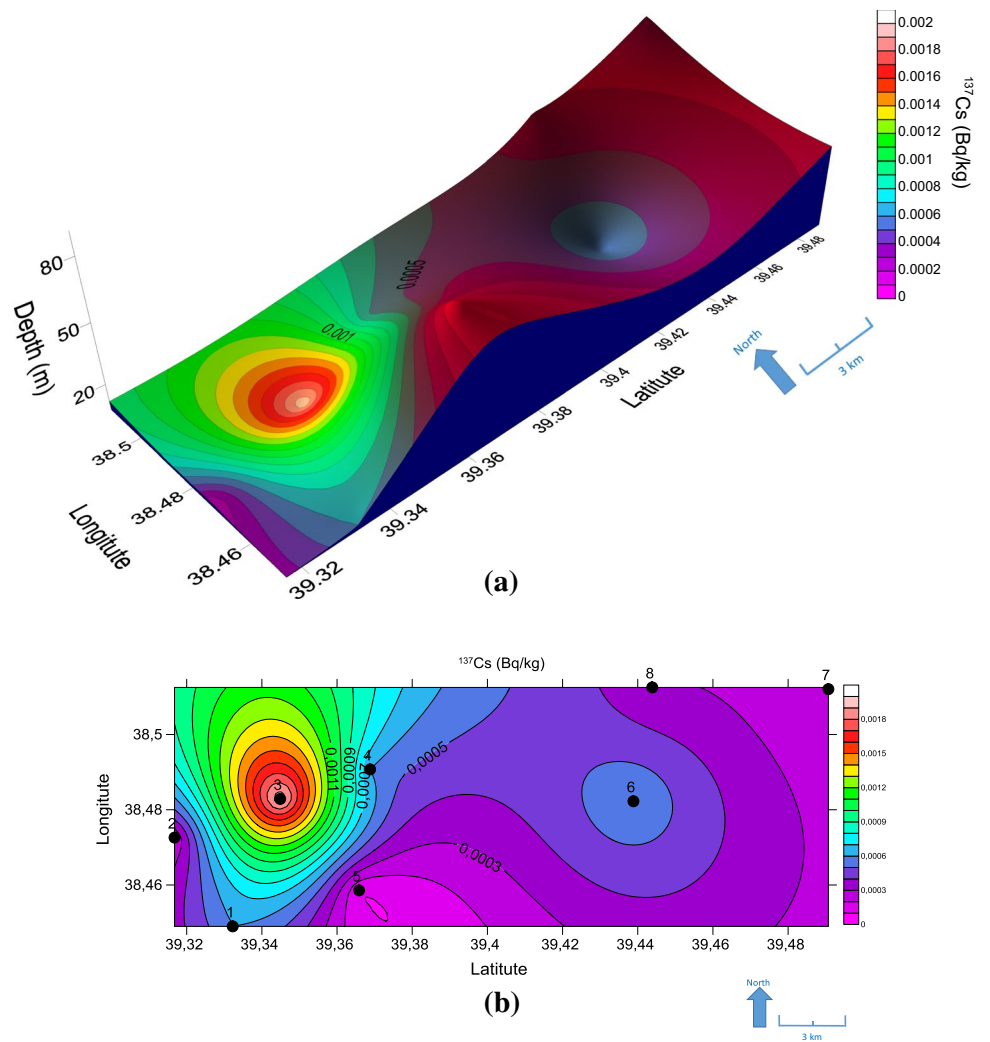
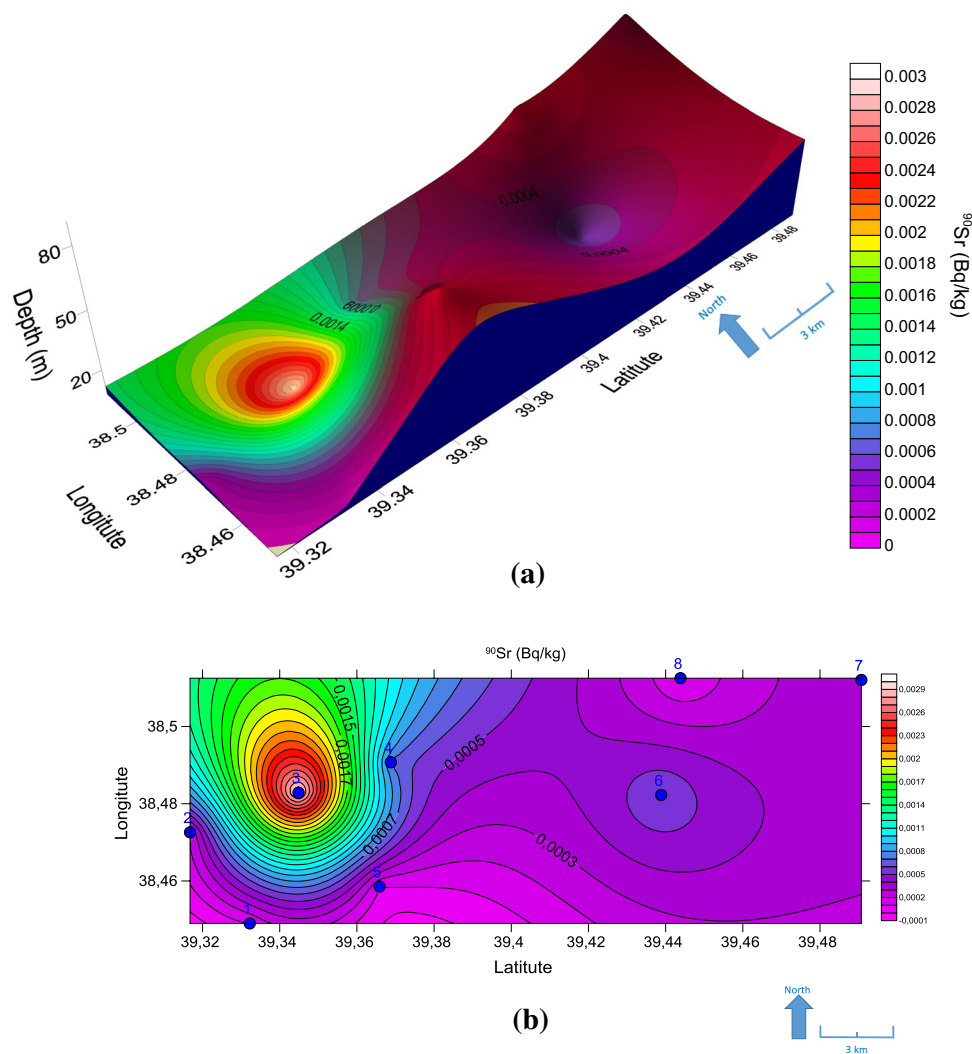


Fig. 16 Bottom sediment, ^{90}Sr **a** three-dimensional and **b** two-dimensional iso-radioactivity diagrams



Acknowledgements A part of this research was supported by TUBITAK-BAYG (The Scientific and Technological Research Council of Turkey-Science People Support Program). We are truly grateful for the excellent management of Editor-in-Chief Zsolt Révay and thank you very much. In addition, we also thank two anonymous referees who have read our article and contributed to its development.

References

- IAEA (2019) International Atomic Energy Agency. <https://www.iaea.org/resources/safety-standards>. Accessed 3 July 2019
- Steinhauser G, Brandl A, Johnson TE (2014) Comparison of the Chernobyl and Fukushima nuclear accidents: a review of the environmental impacts. *Sci Total Environ* 470–471:800–817. <https://doi.org/10.1016/j.scitotenv.2013.10.029>
- Ekberg C, Costa DR, Hedberg M, Jolkkonen M (2018) Nitride fuel for Gen IV nuclear power systems. *J Radioanal Nucl Chem* 318(3):1713–1725. <https://doi.org/10.1007/s10967-018-6316-0>
- Dai G, Levy O, Carrasco N (1996) Cloning and characterization of the thyroid iodide transporter. *Nature* 379(6564):458–460. <https://doi.org/10.1038/379458a0>
- Chino M, Nakayama H, Nagai H, Terada H, Katata G, Yamazawa H (2011) Preliminary estimation of release amounts of ^{131}I and ^{137}Cs accidentally discharged from the Fukushima Daiichi Nuclear power plant into the atmosphere. *J Nucl Sci Technol* 48(7):11134. <https://doi.org/10.3327/jnst.48.1129>
- Navarrete JM, Espinosa G, Golarri JI, Muller G, Zuniga MA, Camacho M (2014) Marine sediments as a radioactive pollution repository in the world. *J Radioanal Nucl Chem* 299(1):843–847. <https://doi.org/10.1007/s10967-013-2707-4>
- Morino Y, Ohara T, Nishizawa M (2011) Atmospheric behavior, deposition, and budget of radioactive materials from the Fukushima Daiichi nuclear power plant in March 2011. *Geophys Res Lett.* <https://doi.org/10.1029/2011gl048689>
- Aoyama M (2018) Long-range transport of radiocesium derived from global fallout and the Fukushima accident in the Pacific Ocean since 1953 through 2017 Part I: source term and surface transport. *J Radioanal Nucl Chem* 318(3):1519–1542. <https://doi.org/10.1007/s10967-018-6244-z>
- Inomata Y, Aoyama M, Tsubono T, Tsumune D, Kumamoto Y, Nagai H, Yamagata T, Kajino M, Tanaka YT, Sekiyama TT, Oka E, Yamada M (2018) Estimate of Fukushima-derived radiocesium in the North Pacific Ocean in summer 2012. *J Radioanal Nucl Chem* 318(3):1587–1596. <https://doi.org/10.1007/s10967-018-6249-7>

10. Koarashi J, Atarashi-Andoh M (2019) Low Cs-137 retention capability of organic layers in Japanese forest ecosystems affected by the Fukushima nuclear accident. *J Radioanal Nucl Chem* 320(1):179–191. <https://doi.org/10.1007/s10967-019-06435-7>
11. Mahmood ZUW, Yii MW, Khalid MA, Yusof MA, Mohamed N (2018) Marine radioactivity of Cs-134 and Cs-137 in the Malaysian Economic Exclusive Zone after the Fukushima accident. *J Radioanal Nucl Chem* 318(3):2165–2172. <https://doi.org/10.1007/s10967-018-6306-2>
12. Nagakawa Y, Uemoto M, Kurosawa T, Shutoh K, Hasegawa H, Sakurai N, Harada E (2019) Comparison of radioactive and stable cesium uptake in aquatic macrophytes affected by the Fukushima Dai-ichi Nuclear Power Plant accident. *J Radioanal Nucl Chem* 319(1):185–196. <https://doi.org/10.1007/s10967-018-6304-4>
13. Paterne M, Evrard O, Hatte C, Lacey PJ, Nouet J, Onda Y (2019) Radiocarbon and radiocesium in litter fall at Kawamata, similar to 45 km NW from the Fukushima Dai-ichi nuclear power plant (Japan). *J Radioanal Nucl Chem* 319(3):1093–1101. <https://doi.org/10.1007/s10967-018-6360-9>
14. Thiessen KM, Thorne MC, Maul PR, Prohl G, Wheeler HS (1999) Modelling radionuclide distribution and transport in the environment. *Environ Pollut* 100(1–3):151–177. [https://doi.org/10.1016/S0269-7491\(99\)00090-1](https://doi.org/10.1016/S0269-7491(99)00090-1)
15. Tsumune D, Tsubono T, Aoyama M, Hirose K (2012) Distribution of oceanic Cs-137 from the Fukushima Dai-ichi Nuclear Power Plant simulated numerically by a regional ocean model. *J Environ Radioact* 111:100–108. <https://doi.org/10.1016/j.jenvrad.2011.10.007>
16. Steinhäuser G, Saey PRJ (2016) Cs-137 in the meat of wild boars: a comparison of the impacts of Chernobyl and Fukushima. *J Radioanal Nucl Chem* 307(3):1801–1806. <https://doi.org/10.1007/s10967-015-4417-6>
17. Kitto ME, Menia TA, Haines DK, Beach SE, Bradt CJ, Fielman EM, Syed UF, Semkow TM, Bari A, Khan AJ (2013) Airborne gamma-ray emitters from Fukushima detected in New York State. *J Radioanal Nucl Chem* 296(1):49–56. <https://doi.org/10.1007/s10967-012-2043-0>
18. Lee SH, Heo DH, Kang HB, Oh PJ, Lee JM, Park TS, Lee KB, Oh JS, Suh JK (2013) Distribution of I-131, Cs-134, Cs-137 and Pu-239, Pu-240 concentrations in Korean rainwater after the Fukushima nuclear power plant accident. *J Radioanal Nucl Chem* 296(2):727–731. <https://doi.org/10.1007/s10967-012-2030-5>
19. Zhang WH, Friese J, Ungar K (2013) The ambient gamma dose rate and the inventory of fission products estimations with the soil samples collected at Canadian embassy in Tokyo during Fukushima nuclear accident. *J Radioanal Nucl Chem* 296(1):69–73. <https://doi.org/10.1007/s10967-012-2040-3>
20. Katata G, Chino M, Kobayashi T, Terada H, Ota M, Nagai H, Kajino M, Draxler R, Hort MC, Malo A, Torii T, Sanada Y (2015) Detailed source term estimation of the atmospheric release for the Fukushima Daiichi Nuclear Power Station accident by coupling simulations of an atmospheric dispersion model with an improved deposition scheme and oceanic dispersion model. *Atmos Chem Phys* 15(2):1029–1070. <https://doi.org/10.5194/acp-15-1029-2015>
21. Melgunov M, Pokhilenko N, Strakhovenko V, Sukhorukov F, Chuguevskii A (2012) Fallout traces of the Fukushima NPP accident in southern West Siberia (Novosibirsk, Russia). *Environ Sci Pollut Res* 19(4):1323–1325
22. MEXT Culture S, Science and Technology JM of E MEXT, Japan Ministry of Education (2011) Reading of environmental radioactivity level by prefecture <http://www.mext.go.jp/>. Accessed 10 Oct 2011
23. García FP, García MF (2012) Traces of fission products in southeast Spain after the Fukushima nuclear accident. *J Environ Radioact* 114:146–151
24. Terada H, Katata G, Chino M, Nagai H (2012) Atmospheric discharge and dispersion of radionuclides during the Fukushima Dai-ichi Nuclear Power Plant accident. Part II: verification of the source term and analysis of regional-scale atmospheric dispersion. *J Environ Radioact* 112:141–154
25. Povinec P, Hirose K, Aoyama M (2013) Fukushima accident: radioactivity impact on the environment. Newnes
26. Imanaka T, Hayashi G, Endo S (2015) Comparison of the accident process, radioactivity release and ground contamination between Chernobyl and Fukushima-1. *J Radiat Res* 56(suppl_1):i56–i61
27. Chino M, Nakayama H, Nagai H, Terada H, Katata G, Yamazawa H (2011) Preliminary estimation of release amounts of ¹³¹I and ¹³⁷Cs accidentally discharged from the Fukushima Daiichi nuclear power plant into the atmosphere. *J Nucl Sci Technol* 48(7):1129–1134
28. Sholkovitz ER (1983) The geochemistry of plutonium in fresh and marine water environments. *Earth Sci Rev* 19(2):95–161. [https://doi.org/10.1016/0012-8252\(83\)90029-6](https://doi.org/10.1016/0012-8252(83)90029-6)
29. Gauthier-Lafaye F, Holliger P, Blanc PL (1996) Natural fission reactors in the Franceville basin, Gabon: a review of the conditions and results of a “critical event” in a geologic system. *Geochim Cosmochim Acta* 60(23):4831–4852. [https://doi.org/10.1016/S0016-7037\(96\)00245-1](https://doi.org/10.1016/S0016-7037(96)00245-1)
30. Tsumune D, Aoyama M, Hirose K (2003) Behavior of ¹³⁷Cs concentrations in the North Pacific in an ocean general circulation model. *J Geophys Res C Oceans* 108(8):11–18
31. Matiullah A, Ahad A, ur Rehman S, ur Rehman S, Faheem M (2004) Measurement of radioactivity in the soil of Bahawalpur division, Pakistan. *Radiat Prot Dosimet* 112(3):443–447. <https://doi.org/10.1093/rpd/nch409>
32. Kùlahcı F, Şen Z (2008) Multivariate statistical analyses of artificial radionuclides and heavy metals contaminations in deep mud of Keban Dam Lake, Turkey. *Appl Radiat Isot* 66(2):236–246. <https://doi.org/10.1016/j.apradiso.2007.08.014>
33. Ferrand E, Eyrolle F, Radakovitch O, Provansal M, Dufour S, Vella C, Raccasi G, Gurriaran R (2012) Historical levels of heavy metals and artificial radionuclides reconstructed from overbank sediment records in lower Rhône River (South-East France). *Geochim Cosmochim Acta* 82:163–182. <https://doi.org/10.1016/j.gca.2011.11.023>
34. Honda MC, Aono T, Aoyama M, Hamajima Y, Kawakami H, Kitamura M, Masumoto Y, Miyazawa Y, Takigawa M, Saino T (2012) Dispersion of artificial caesium-134 and -137 in the western North Pacific one month after the Fukushima accident. *Geochim J* 46(4):e1–e9
35. Wallace SH, Shaw S, Morris K, Small JS, Fuller AJ, Burke IT (2012) Effect of groundwater pH and ionic strength on strontium sorption in aquifer sediments: implications for ⁹⁰Sr mobility at contaminated nuclear sites. *Appl Geochem* 27(8):1482–1491. <https://doi.org/10.1016/j.apgeochem.2012.04.007>
36. Ashraf MA, Khan AM, Ahmad M, Akib S, Balkhair KS, Bakar NKA (2014) Release, deposition and elimination of radiocesium ¹³⁷Cs in the terrestrial environment. *Environ Geochem Health* 36(6):1165–1190. <https://doi.org/10.1007/s10653-014-9620-9>
37. Topcuoglu S, Turer A, Gungor N, Kirbasoglu C (2003) Monitoring of anthropogenic and natural radionuclides and gamma absorbed dose rates in eastern Anatolia. *J Radioanal Nucl Chem* 258(3):547–550. <https://doi.org/10.1023/b:jrncl.0000011750.97805.78>
38. Garraffo ZD, Kim HC, Mehra A, Spindler T, Rivin I, Tolman HL (2016) Modeling of ¹³⁷Cs as a tracer in a regional

- model for the western Pacific, after the Fukushima-Daiichi nuclear power plant accident of March 2011. *Weather Forecast* 31(2):553–579. <https://doi.org/10.1175/WAF-D-13-00101.1>
39. Baklanov A, Sørensen JH (2001) Parameterisation of radionuclide deposition in atmospheric long-range transport modelling. *Phys Chem Earth Part B* 26(10):787–799. [https://doi.org/10.1016/S1464-1909\(01\)00087-9](https://doi.org/10.1016/S1464-1909(01)00087-9)
 40. Bailly du Bois P, Dumas F (2005) Fast hydrodynamic model for medium- and long-term dispersion in seawater in the English Channel and southern North Sea, qualitative and quantitative validation by radionuclide tracers. *Ocean Model Online* 9(2):169–210. <https://doi.org/10.1016/j.ocemod.2004.07.004>
 41. Bocquet M (2005) Reconstruction of an atmospheric tracer source using the principle of maximum entropy. I: Theory. *Q J R Meteorol Soc* 131(610 B):2191–2208. <https://doi.org/10.1256/qj.04.67>
 42. Bocquet M (2005) Grid resolution dependence in the reconstruction of an atmospheric tracer source. *Nonlinear Process Geophys* 12(2):219–234
 43. Krysta M, Bocquet M (2007) Source reconstruction of an accidental radionuclide release at European scale. *Q J R Meteorol Soc* 133(623):529–544. <https://doi.org/10.1002/qj.3>
 44. Estournel C, Bosc E, Bocquet M, Ulses C, Marsaleix P, Winiarek V, Osvald I, Nguyen C, Duhaut T, Lyard F, Michaud H, Auclair F (2012) Assessment of the amount of cesium-137 released into the Pacific Ocean after the Fukushima accident and analysis of its dispersion in Japanese coastal waters. *J Geophys Res C Oceans*. <https://doi.org/10.1029/2012jc007933>
 45. Terada H, Katata G, Chino M, Nagai H (2012) Atmospheric discharge and dispersion of radionuclides during the Fukushima Dai-ichi Nuclear Power Plant accident. Part II: verification of the source term and analysis of regional-scale atmospheric dispersion. *J Environ Radioact* 112:141–154. <https://doi.org/10.1016/j.jenvrad.2012.05.023>
 46. Winiarek V, Bocquet M, Saunier O, Mathieu A (2012) Estimation of errors in the inverse modeling of accidental release of atmospheric pollutant: Application to the reconstruction of the cesium-137 and iodine-131 source terms from the Fukushima Daiichi power plant. *J Geophys Res D Atmos*. <https://doi.org/10.1029/2011jd016932>
 47. Christoudias T, Lelieveld J (2013) Modelling the global atmospheric transport and deposition of radionuclides from the Fukushima Dai-ichi nuclear accident. *Atmos Chem Phys* 13(3):1425–1438. <https://doi.org/10.5194/acp-13-1425-2013>
 48. Cunha ILL, Figueira RCL, Saito RT (1999) Application of radiochemical methods and dispersion model in the study of environmental pollution in Brazil. *J Radioanal Nucl Chem* 239(3):477–482. <https://doi.org/10.1007/bf02349054>
 49. El Mrabet R, Abril JM, Manjon G, Tenorio RG (2004) Experimental and modeling study of Am-241 uptake by suspended matter in freshwater environment from southern Spain. *J Radioanal Nucl Chem* 261(1):137–144. <https://doi.org/10.1023/B:JRNC.0000030947.24584.dc>
 50. Jones KA, Prosser SL (1997) A comparison of Pu239 + 240 post-mortem measurements with estimates based on current ICRP models. *J Radioanal Nucl Chem* 226(1–2):129–133. <https://doi.org/10.1007/bf02063636>
 51. Kim S, Min BI, Park K, Yang BM, Kim J, Suh KS (2018) Evaluation of radionuclide concentration in agricultural food produced in Fukushima Prefecture following Fukushima accident using a terrestrial food chain model. *J Radioanal Nucl Chem* 316(3):1091–1098. <https://doi.org/10.1007/s10967-018-5779-3>
 52. Kumar A, Rout S, Chopra MK, Mishra DG, Singhal RK, Ravi PM, Tripathi RM (2014) Modeling of Cs-137 migration in cores of marine sediments of Mumbai Harbor Bay. *J Radioanal Nucl Chem* 301(2):615–626. <https://doi.org/10.1007/s10967-014-3116-z>
 53. Perianez R, Pascual-Granged A (2007) A rapid response model for simulating radioactivity dispersion in the Strait of Gibraltar. *J Radioanal Nucl Chem* 274(2):301–306. <https://doi.org/10.1007/s10967-007-1115-z>
 54. Sert I, Eftelioglu M, Ozel FE (2017) Historical evolution of heavy metal pollution and recent records in Lake Karagol sediment cores using Pb-210 models, western Turkey. *J Radioanal Nucl Chem* 314(3):2155–2169. <https://doi.org/10.1007/s10967-017-5627-x>
 55. Sert I, Ozel FE, Yaprak G, Eftelioglu M (2016) Determination of the latest sediment accumulation rates and pattern by performing Pb-210 models and Cs-137 technique in the Lake Bafa, Mugla, Turkey. *J Radioanal Nucl Chem* 307(1):313–323. <https://doi.org/10.1007/s10967-015-4234-y>
 56. Tsumune D, Aoyama M, Hirose K, Maruyama K, Nakashiki N (2001) Calculation of artificial radionuclides in the ocean by an ocean general circulation model. *J Radioanal Nucl Chem* 248(3):777–783. <https://doi.org/10.1023/a:1010665300905>
 57. Ueda S, Kondo K, Inaba J, Kutsukake H, Nakata K (2006) Development and application of an eco-hydrodynamic model for radionuclides in a brackish lake: case study of Lake Obuchi, Japan, bordered by nuclear fuel cycling facilities. *J Radioanal Nucl Chem* 268(2):261–273. <https://doi.org/10.1556/jrnc.268.2006.2.13>
 58. Yamamoto K, Tagami K, Uchida S, Ishii N (2015) Model estimation of Cs-137 concentration change with time in seawater and sediment around the Fukushima Daiichi Nuclear Power Plant site considering fast and slow reactions in the seawater-sediment systems. *J Radioanal Nucl Chem* 304(2):867–881. <https://doi.org/10.1007/s10967-014-3897-0>
 59. Possolo A (2013) Five examples of assessment and expression of measurement uncertainty. *Appl Stoch Models Bus Ind* 29(1):1–18. <https://doi.org/10.1002/asmb.1947>
 60. Evangelou E, Maroulas V (2017) Sequential empirical Bayes method for filtering dynamic spatiotemporal processes. *Spat Stat* 21:114–129. <https://doi.org/10.1016/j.spasta.2017.06.006>
 61. Marley NA, Gaffney JS, Orlandini KA, Cunningham MM (1993) Evidence for radionuclide transport and mobilization in a shallow, sandy aquifer. *Environ Sci Technol* 27(12):2456–2461. <https://doi.org/10.1021/es00048a022>
 62. Pollanen R, Valkama I, Toivonen H (1997) Transport of radioactive particles from the Chernobyl accident. *Atmos Environ* 31(21):3575–3590. [https://doi.org/10.1016/s1352-2310\(97\)00156-8](https://doi.org/10.1016/s1352-2310(97)00156-8)
 63. Kaste JM, Heimsath AM, Bostick BC (2007) Short-term soil mixing quantified with fallout radionuclides. *Geology* 35(3):243–246. <https://doi.org/10.1130/g23355a.1>
 64. Hirose K (2012) 2011 Fukushima Dai-ichi nuclear power plant accident: summary of regional radioactive deposition monitoring results. *J Environ Radioact* 111:13–17. <https://doi.org/10.1016/j.jenvrad.2011.09.003>
 65. Stohl A, Seibert P, Wotawa G, Arnold D, Burkhart JF, Eckhardt S, Tapia C, Vargas A, Yasunari TJ (2012) Xenon-133 and caesium-137 releases into the atmosphere from the Fukushima Dai-ichi nuclear power plant: determination of the source term, atmospheric dispersion, and deposition. *Atmos Chem Phys* 12(5):2313–2343. <https://doi.org/10.5194/acp-12-2313-2012>
 66. Kılıhçı F, Şen Z (2007) Spatial dispersion modeling of 90 Sr by point cumulative semivariogram at Keban Dam Lake, Turkey. *Appl Radiat Isot* 65(9):1070–1077
 67. Helton JC (1994) Treatment of uncertainty in performance assessments for complex systems. *Risk Anal* 14(4):483–511. <https://doi.org/10.1111/j.1539-6924.1994.tb00266.x>

68. Reason J (1990) The contribution of latent human failures to the breakdown of complex systems. *Philos Trans R Soc Lond B Biol Sci* 327(1241):475–484. <https://doi.org/10.1098/rstb.1990.0090>
69. Schulz TL (2006) Westinghouse AP1000 advanced passive plant. *Nucl Eng Des* 236(14–16):1547–1557. <https://doi.org/10.1016/j.nucengdes.2006.03.049>
70. Stohl A, Seibert P, Wotawa G, Arnold D, Burkhart JF, Eckhardt S, Tapia C, Vargas A, Yasunari TJ (2012) Xenon-133 and caesium-137 releases into the atmosphere from the Fukushima Dai-ichi nuclear power plant: determination of the source term, atmospheric dispersion, and deposition. *Atmos Chem Phys* 12(5):2313–2343. <https://doi.org/10.5194/acp-12-2313-2012>
71. Yasunari TJ, Stohl A, Hayano RS, Burkhart JF, Eckhardt S, Yasunari T (2011) Cesium-137 deposition and contamination of Japanese soils due to the Fukushima nuclear accident. *Proc Natl Acad Sci USA* 108(49):19530–19534. <https://doi.org/10.1073/pnas.1112058108>
72. Martinho M, Freitas MC (2009) Spatial regression analysis between air pollution and childhood leukaemia in Portugal. *J Radioanal Nucl Chem* 281(2):175–179. <https://doi.org/10.1007/s10967-009-0124-5>
73. Menezes MAdBC, Jacimovic R, Pereira C (2015) Spatial distribution of neutron flux in geological larger sample analysis at CDTN/CNEN, Brazil. *J Radioanal Nucl Chem* 306(3):611–616. <https://doi.org/10.1007/s10967-015-4226-y>
74. Şen Z (2009) *Spatial modeling principles in Earth sciences*. Springer, Berlin
75. Zoran M, Savastru R, Savastru D (2012) Ground based radon (Rn-222) observations in Bucharest, Romania and their application to geophysics. *J Radioanal Nucl Chem* 293(3):877–888. <https://doi.org/10.1007/s10967-012-1761-7>
76. Zoran MA, Dida MR, Zoran A, Zoran LF, Dida A (2013) Outdoor (222)Radon concentrations monitoring in relation with particulate matter levels and possible health effects. *J Radioanal Nucl Chem* 296(3):1179–1192. <https://doi.org/10.1007/s10967-012-2259-z>
77. Fowler SW, Buat-Menard P, Yokoyama Y, Ballestra S, Holm E, Nguyen HV (1987) Rapid removal of Chernobyl fallout from Mediterranean surface waters by biological activity. *Nature* 329(6134):56–58
78. Cressie N (1991) *Statistics for spatial data*. Wiley, Hoboken
79. Zelt CA, Smith RB (1992) Seismic travelttime inversion for 2-D crustal velocity structure. *Geophys J Int* 108(1):16–34. <https://doi.org/10.1111/j.1365-246X.1992.tb00836.x>
80. Braun K, Böhnke F, Stark T (2012) Three-dimensional representation of the human cochlea using micro-computed tomography data: presenting an anatomical model for further numerical calculations. *Acta Oto-Laryngol* 132(6):603–613. <https://doi.org/10.3109/00016489.2011.653670>
81. Tanaka K, Sakaguchi A, Kanai Y, Tsuruta H, Shinohara A, Takahashi Y (2013) Heterogeneous distribution of radiocesium in aerosols, soil and particulate matters emitted by the Fukushima Daiichi Nuclear Power Plant accident: retention of micro-scale heterogeneity during the migration of radiocesium from the air into ground and river systems. *J Radioanal Nucl Chem* 295(3):1927–1937. <https://doi.org/10.1007/s10967-012-2160-9>
82. Wieland E, Mace N, Daehn R, Kunz D, Tits J (2010) Macro- and micro-scale studies on U(VI) immobilization in hardened cement paste. *J Radioanal Nucl Chem* 286(3):793–800. <https://doi.org/10.1007/s10967-010-0742-y>
83. Diniz-Filho JAF, Bini LM, Hawkins BA (2003) Spatial autocorrelation and red herrings in geographical ecology. *Glob Ecol Biogeogr* 12(1):53–64. <https://doi.org/10.1046/j.1466-822X.2003.00322.x>
84. Halley E (1753) An historical account of the trade winds, and monsoons, observable in the seas between and near the tropicks, with an attempt to assign the physical cause of the said winds. *Philos Trans* (1683-1775) 16:153–168
85. Student (1907) On the error of counting with a haemocytometer. *Biometrika* 5:351–360
86. Lawrie JA (1962) The spatial distribution of rapid geomagnetic fluctuations. *Geophys J Int* 7(1):102–110. <https://doi.org/10.1111/j.1365-246X.1962.tb02255.x>
87. Ernst WG (1965) Mineral parageneses in franciscan metamorphic rocks, Panoche Pass, California. *Bull Geol Soc Am* 76(8):879–914. [https://doi.org/10.1130/0016-7606\(1965\)76%5b879:mpimfr%5d2.0.co;2](https://doi.org/10.1130/0016-7606(1965)76%5b879:mpimfr%5d2.0.co;2)
88. Lomnitz C (1966) Statistical prediction of earthquakes. *Rev Geophys* 4(3):377–393. <https://doi.org/10.1029/RG004i003p00377>
89. Strick E (1967) The determination of Q, dynamic viscosity and transient creep curves from wave propagation measurements. *Geophys J R Astron Soc* 13(1–3):197–218. <https://doi.org/10.1111/j.1365-246X.1967.tb02154.x>
90. Becchi I, Caporali E, Castellani L, Palmisano E, Castelli F (1995) Hydrological control of flooding: Tuscany. *Surv Geophys* 16(2):227–252. <https://doi.org/10.1007/BF00665781>
91. Coroniti FV (1973) The ring current and magnetic storms. *Radio Sci* 8(11):1007–1011. <https://doi.org/10.1029/RS008i011p01007>
92. Mo T, Suttle AD, Sackett WM (1973) Uranium concentrations in marine sediments. *Geochim Cosmochim Acta* 37(1):35–51. [https://doi.org/10.1016/0016-7037\(73\)90242-1](https://doi.org/10.1016/0016-7037(73)90242-1)
93. Wing AA, Emanuel K, Holloway CE, Muller C (2017) Convective self-aggregation in numerical simulations: a review. *Surv Geophys* 38(6):1173–1197. <https://doi.org/10.1007/s10712-017-9408-4>
94. Filho CRdF, Nunes AR, Leite EP, Monteiro LVS, Xavier RP (2007) Spatial analysis of airborne geophysical data applied to geological mapping and mineral prospecting in the Serra Leste Region, Carajás Mineral Province, Brazil. *Surv Geophys* 28(5–6):377–405. <https://doi.org/10.1007/s10712-008-9031-5>
95. Slater L (2007) Near surface electrical characterization of hydraulic conductivity: from petrophysical properties to aquifer geometries—a review. *Surv Geophys* 28(2–3):169–197. <https://doi.org/10.1007/s10712-007-9022-y>
96. Tenzer R, Hirt C, Claessens S, Novák P (2015) Spatial and spectral representations of the geoid-to-quasigeoid correction. *Surv Geophys* 36(5):627–658. <https://doi.org/10.1007/s10712-015-9337-z>
97. Külahcı F, Şen Z (2014) On the Correction of spatial and statistical uncertainties in systematic measurements of ²²²Rn for earthquake prediction. *Surv Geophys* 35(2):449–478. <https://doi.org/10.1007/s10712-013-9273-8>
98. Külahcı F, Şen Z (2009) Potential utilization of the absolute point cumulative semivariogram technique for the evaluation of distribution coefficient. *J Hazard Mater* 168(2–3):1387–1396. <https://doi.org/10.1016/j.jhazmat.2009.03.027>
99. Matheron G (1963) Principles of geostatistics. *Econ Geol* 58(8):1246–1266. <https://doi.org/10.2113/gsecongeo.58.8.1246>
100. Şen Z (1998) Point cumulative semivariogram for identification of heterogeneities in regional seismicity of Turkey. *Math Geol* 30(7):767–787
101. Külahcı F, Şen Z (2009) Spatio-temporal modeling of ²¹⁰Pb transportation in lake environments. *J Hazard Mater* 165(1–3):525–532. <https://doi.org/10.1016/j.jhazmat.2008.10.026>
102. Acar R, Sengul S (2012) The estimation of average areal snowfall by conventional methods and the percentage weighting polygon method in the Northeast Anatolia region, Turkey. *Energy Educ Sci Technol Part A Energy Sci Res* 29(1):11–22
103. Tarawneh Q, Şen Z (2012) Spatial climate variation pattern and regional prediction of rainfall in Jordan. *Water Environ J* 26(2):252–260. <https://doi.org/10.1111/j.1747-6593.2011.00284.x>

104. Anderson OL (1986) Properties of iron at the Earth's core conditions. *Geophys J Int* 84(3):561–579. <https://doi.org/10.1111/j.1365-246X.1986.tb04371.x>
105. Dubois M, Royer JJ, Weisbrod A, Shtuka A (1993) Reconstruction of low-temperature binary phase diagrams using a constrained least squares method: application to the H₂O–CsCl system. *Eur J Mineral* 5(6):1145–1152. <https://doi.org/10.1127/ejm/5/6/1145>
106. Nagahara H, Kushiro I, Mysen BO (1994) Evaporation of olivine: low pressure phase relations of the olivine system and its implication for the origin of chondritic components in the solar nebula. *Geochim Cosmochim Acta* 58(8):1951–1963. [https://doi.org/10.1016/0016-7037\(94\)90426-X](https://doi.org/10.1016/0016-7037(94)90426-X)
107. Sato H, Niizato T, Amano K, Tanaka S, Aoki K (2013) Investigation and research on depth distribution in soil of radionuclides released by the TEPCO Fukushima Dai-ichi Nuclear Power Plant accident, pp 277–282. <https://doi.org/10.1557/opl.2013.393>
108. Sağıroğlu A, Çetindağ B (1995) Hazar Gölü'nün Kürk ve Mogal derelerinden kaynaklanan şiltleşmesi, I. Hazar Gölü ve Çevresi Sempozyumu, Çağ Ofset, Elazığ, pp 33–39
109. Sungurlu O, Perinçek D, Kurt G, Tuna E, Dülger S, Çelikdemir E, Naz H (1985) Geology of the Elazığ-Hazar-Palu area. *Bull Turk Assoc Pet Geol* 29:83–191
110. Eriş KK, Ön SA, Çağatay MN, Ülgen UB, Ön ZB, Gürocak Z, Arslan TN, Akkoca DB, Damcı E, İnceöz M (2018) Late Pleistocene to Holocene paleoenvironmental evolution of Lake Hazar, Eastern Anatolia, Turkey. *Quatern Int* 486:4–16
111. Moreno DG, Hubert-Ferrari A, Moernaut J, Fraser J, Boes X, Van Daele M, Avsar U, Çağatay N, De Batist M (2011) Structure and recent evolution of the Hazar Basin: a strike-slip basin on the East Anatolian Fault, Eastern Turkey. *Basin Res* 23(2):191–207
112. Hempton M, Dunne L, Dewey J (1983) Sedimentation in an active strike-slip basin, southeastern Turkey. *J Geol* 91(4):401–412
113. Aközcan S, Külahcı F, Mercan Y (2018) A suggestion to radiological hazards characterization of 226Ra, 232Th, 40K and 137Cs: spatial distribution modelling. *J Hazard Mater* 353:476–489
114. Aközcan S, Külahcı F (2018) Descriptive statistics and risk assessment for the control of seasonal pollutant effects of 210Po and 210Pb in coastal waters (Çanakkale, Turkey). *J Radioanal Nucl Chem* 315(2):285–292
115. Şen Z (1989) Cumulative semivariogram models of regionalized variables. *Math Geol* 21(8):891–903. <https://doi.org/10.1007/BF00894454>
116. Şen Z (1992) Standard cumulative semivariograms of stationary stochastic processes and regional correlation. *Math Geol* 24(4):417–435. <https://doi.org/10.1007/BF00891272>
117. Davis JC, Sampson RJ (1986) *Statistics and data analysis in geology*, vol 646. Wiley, New York
118. Turalioglu FS, Bayraktar H (2005) Assessment of regional air pollution distribution by point cumulative semivariogram method at Erzurum urban center, Turkey. *Stoch Environ Res Risk Assess* 19(1):41–47. <https://doi.org/10.1007/s00477-004-0203-7>
119. Külahcı F, Şen Z, Kazanç S (2008) Cesium concentration spatial distribution modeling by point cumulative semivariogram. *Water Air Soil Pollut* 195(1–4):151–160. <https://doi.org/10.1007/s11270-008-9734-8>
120. Özger M, Şen Z (2007) Triple diagram method for the prediction of wave height and period. *Ocean Eng* 34(7):1060–1068. <https://doi.org/10.1016/j.oceaneng.2006.05.006>
121. Suursaar Ü, Kullas T (2009) Decadal variations in wave heights off Cape Kelba, Saaremaa Island, and their relationships with changes in wind climate. *Oceanologia* 51(1):39–61. <https://doi.org/10.5697/oc.51-1.039>
122. Zaitseva-Pärnaste I, Suursaar Ü, Kullas T, Lapimaa S, Soomere T (2009) Seasonal and long-term variations of wave conditions in the northern baltic sea. *J Coast Res (SPEC. ISSUE 56)*:277–281
123. Vanem E (2011) Long-term time-dependent stochastic modelling of extreme waves. *Stoch Environ Res Risk Assess* 25(2):185–209. <https://doi.org/10.1007/s00477-010-0431-y>
124. Sharma LK, Ghosh AK, Nair RN, Chopra M, Sunny F, Puranik VD (2014) Inverse modeling for aquatic source and transport parameters identification and its application to Fukushima nuclear accident. *Environ Model Assess* 19(3):193–206. <https://doi.org/10.1007/s10666-013-9391-1>
125. Povinec PP, Hirose K, Aoyama M (2013) Fukushima accident: radioactivity impact on the environment. Elsevier Inc., Amsterdam. <https://doi.org/10.1016/C2012-0-06837-8>
126. Minoura K, Yamada T, Hirano SI, Sugihara S (2014) Movement of radiocaesium fallout released by the 2011 Fukushima nuclear accident. *Nat Hazards* 73(3):1843–1862. <https://doi.org/10.1007/s11069-014-1171-y>
127. Perriáñez R, Bezhenar R, Brovchenko I, Duffa C, Iosjpe M, Jung KT, Kobayashi T, Lamego F, Maderich V, Min BI, Nies H, Osvath I, Outola I, Psaltaki M, Suh KS, de With G (2016) Modelling of marine radionuclide dispersion in IAEA MODARIA program: lessons learnt from the Baltic Sea and Fukushima scenarios. *Sci Total Environ* 569–570:594–602. <https://doi.org/10.1016/j.scitotenv.2016.06.131>
128. Gaucher E, Robelin C, Matray JM, Négrel G, Gros Y, Heitz JF, Vinsot A, Rebours H, Cassagnabère A, Bouchet A (2004) ANDRA underground research laboratory: interpretation of the mineralogical and geochemical data acquired in the Callovian-Oxfordian formation by investigative drilling. *Phys Chem Earth* 29(1):55–77. <https://doi.org/10.1016/j.pce.2003.11.006>
129. Rogers H, Bowers J, Gates-Anderson D (2012) An isotope dilution-precipitation process for removing radioactive cesium from wastewater. *J Hazard Mater* 243:124–129. <https://doi.org/10.1016/j.jhazmat.2012.10.006>
130. Mahura AG, Baklanov AA, Sørensen JH, Parker FL, Novikov V, Brown K, Compton KL (2005) Assessment of potential atmospheric transport and deposition patterns due to Russian pacific fleet operations. *Environ Monit Assess* 101(1–3):261–287. <https://doi.org/10.1007/s10661-005-0295-7>
131. Yamamoto M, Takada T, Nagao S, Koike T, Shimada K, Hoshi M, Zhumadilov K, Shima T, Fukuoka M, Imanaka T, Endo S, Sakaguchi A, Kimura S (2012) An early survey of the radioactive contamination of soil due to the Fukushima Dai-ichi Nuclear Power Plant accident, with emphasis on plutonium analysis. *Geochim J* 46(4):341–353
132. Bopp RF, Simpson HJ, Olsen CR, Trier RM, Kostyk N (1982) Chlorinated hydrocarbons and radionuclide chronologies in sediments of the Hudson River and estuary, New York. *Environ Sci Technol* 16(10):666–676. <https://doi.org/10.1021/es00104a008>
133. Sun H, Semkow TM (1998) Mobilization of thorium, radium and radon radionuclides in ground water by successive alpha-recoils. *J Hydrol* 205(1–2):126–136. [https://doi.org/10.1016/S0022-1694\(97\)00154-6](https://doi.org/10.1016/S0022-1694(97)00154-6)
134. Adriani O, Barbarino GC, Bazilevskaya GA, Bellotti R, Boezio M, Bogomolov EA, Bonechi L, Bonghi M, Bonvicini V, Bottai S, Bruno A, Cafagna F, Campana D, Carlson P, Casolino M, Castellini G, De Pascale MP, De Rosa G, De Simone N, Di Felice V, Galper AM, Grishantseva L, Hofverberg P, Koldashov SV, Krutkov SY, Kvashnin AN, Leonov A, Malvezzi V, Marcelli L, Menn W, Mikhailov VV, Mocchiutti E, Orsi S, Osteria G, Papini P, Pearce M, Picozza P, Ricci M, Ricciarini SB, Simon M, Sparvoli R, Spillantini P, Stozhkov YI, Vacchi A, Vannuccini E, Vasilyev G, Voronov SA, Yurkin YT, Zampa G, Zampa N, Zverev VG (2009) An anomalous positron abundance in cosmic rays with

- energies 1.5–100 GeV. *Nature* 458(7238):607–609. <https://doi.org/10.1038/nature07942>
135. von Blanckenburg F (2005) The control mechanisms of erosion and weathering at basin scale from cosmogenic nuclides in river sediment. *Earth Planet Sci Lett* 237(3–4):462–479. <https://doi.org/10.1016/j.epsl.2005.06.030>
 136. Mohan D, Pittman CU Jr (2007) Arsenic removal from water/wastewater using adsorbents—a critical review. *J Hazard Mater* 142(1–2):1–53. <https://doi.org/10.1016/j.jhazmat.2007.01.006>
 137. Uppala SM, Källberg PW, Simmons AJ, Andrae U, da Costa Bechtold V, Fiorino M, Gibson JK, Haseler J, Hernandez A, Kelly GA, Li X, Onogi K, Saarinen S, Sokka N, Allan RP, Andersson E, Arpe K, Balmaseda MA, Beljaars ACM, van de Berg L, Bidlot J, Bormann N, Caires S, Chevallier F, Dethof A, Dragosavac M, Fisher M, Fuentes M, Hagemann S, Hölm E, Hoskins BJ, Isaksen I, Janssen PAEM, Jenne R, McNally AP, Mahfouf JF, Morcrette JJ, Rayner NA, Saunders RW, Simon P, Sterl A, Trenberth KE, Untch A, Vasiljevic D, Viterbo P, Woollen J (2005) The ERA-40 re-analysis. *Q J R Meteorol Soc* 131(612):2961–3012. <https://doi.org/10.1256/qj.04.176>
 138. Kersting AB, Efurud DW, Finnegan DL, Rokop DJ, Smith DK, Thompson JL (1999) Migration of plutonium in ground water at the Nevada Test Site. *Nature* 397(6714):56–59. <https://doi.org/10.1038/16231>
 139. Chen Z, Montavon G, Ribet S, Guo Z, Robinet JC, David K, Tournassat C, Grambow B, Landesman C (2014) Key factors to understand in situ behavior of Cs in Callovo-Oxfordian clay-rock (France). *Chem Geol* 387(1):47–58. <https://doi.org/10.1016/j.chemgeo.2014.08.008>
 140. Hooper DU, Chapin Iii FS, Ewel JJ, Hector A, Inchausti P, Lavorel S, Lawton JH, Lodge DM, Loreau M, Naeem S, Schmid B, Setälä H, Symstad AJ, Vandermeer J, Wardle DA (2005) Effects of biodiversity on ecosystem functioning: a consensus of current knowledge. *Ecol Monogr* 75(1):3–35
 141. Atkinson PM, Lloyd CD (2010) *geoENV VII—geostatistics for environmental applications*, vol 16. Springer, Berlin
 142. Webster R, Oliver MA (2007) *Geostatistics for environmental scientists*. Wiley, Hoboken
 143. Shapiro SS, Wilk MB, Chen HJ (1968) A comparative study of various tests for normality. *J Am Stat Assoc* 63(324):1343–1372
 144. Zorer OS (2019) Evaluations of environmental hazard parameters of natural and some artificial radionuclides in river water and sediments. *Microchem J* 145:762–766
 145. Ergül HA, Belivermiş M, Kılıç Ö, Topcuoğlu S, Çotuk Y (2013) Natural and artificial radionuclide activity concentrations in surface sediments of Izmit Bay, Turkey. *J Environ Radioact* 126:125–132
 146. Korkulu Z, Özkan N (2013) Determination of natural radioactivity levels of beach sand samples in the black sea coast of Kocaeli (Turkey). *Radiat Phys Chem* 88:27–31
 147. Ibraheim NM, Shawky S, Amer H (1995) Radioactivity levels in Lake Nasser sediments. *Appl Radiat Isot* 46(5):297–299
 148. Otsuka S, Kobayashi T (2013) Sedimentation and remobilization of radiocesium in the coastal area of Ibaraki, 70 km south of the Fukushima Dai-ichi Nuclear Power Plant. *Environ Monit Assess* 185(7):5419–5433
 149. Kang D-J, Chung CS, Kim SH, Kim K-R, Hong GH (1997) Distribution of ¹³⁷Cs and ^{239,240}Pu in the surface waters of the East Sea (Sea of Japan). *Mar Pollut Bull* 35(7–12):305–312
 150. Kim C-K, Kim C-S, Yun J-Y, Kim K-H (1997) Distribution of ³H, ¹³⁷Cs and ^{239,240}Pu in the surface seawater around Korea. *J Radioanal Nucl Chem* 218(1):33
 151. Dulanska S, Remenec B, Matel L, Galanda D, Molnar A (2011) Pre-concentration and determination of Sr-90 in radioactive wastes using solid phase extraction techniques. *J Radioanal Nucl Chem* 288(3):705–708. <https://doi.org/10.1007/s10967-011-1019-9>
 152. Ligeró R, Ramos-Lerate I, Barrera M, Casas-Ruiz M (2001) Relationships between sea-bed radionuclide activities and some sedimentological variables. *J Environ Radioact* 57(1):7–19
 153. Shishkina EA, Pryakhin EA, Popova IY, Osipov DI, Tikhova Y, Andreyev S, Shaposhnikova I, Egoreichenkov E, Styazhkina E, Deryabina LV (2016) Evaluation of distribution coefficients and concentration ratios of ⁹⁰Sr and ¹³⁷Cs in the Techa River and the Miass River. *J Environ Radioact* 158:148–163
 154. Darko G, Faanu A, Akoto O, Acheampong A, Goode EJ, Gyamfi O (2015) Distribution of natural and artificial radioactivity in soils, water and tuber crops. *Environ Monit Assess* 187(6):339
 155. Fallah M, Jahangiri S, Janadeleh H, Kameli MA (2019) Distribution and risk assessment of radionuclides in river sediments along the Arvand River, Iran. *Microchem J* 146:1090–1094. <https://doi.org/10.1016/j.microc.2019.02.028>
 156. Matheron G (1970) Random functions and their application in geology. In: *Geostatistics*. Springer, pp 79–87
 157. Isaaks E, Srivastava R (1989) *Applied geostatistics*. Oxford University Press, New York
 158. Journel AG, Huijbregts CJ (1978) *Mining geostatistics*. Academic Press, New York
 159. Illian J, Penttinen A, Stoyan H, Stoyan D (2008) *Statistical analysis and modelling of spatial point patterns*. Wiley Blackwell, Hoboken. <https://doi.org/10.1002/9780470725160>
 160. Watanabe T, Tsuchiya N, Oura Y, Ebihara M, Inoue C, Hirano N, Yamada R, Yamasaki SI, Okamoto A, Nara FW, Nunohara K (2012) Distribution of artificial radionuclides (^{110m}Ag, ^{129m}Te, ¹³⁴Cs, ¹³⁷Cs) in surface soils from Miyagi Prefecture, northeast Japan, following the 2011 Fukushima Dai-ichi nuclear power plant accident. *Geochem J* 46(4):279–285
 161. Özsoy E, Ünlüata Ü (1997) Oceanography of the Black Sea: a review of some recent results. *Earth Sci Rev* 42(4):231–272. [https://doi.org/10.1016/S0012-8252\(97\)81859-4](https://doi.org/10.1016/S0012-8252(97)81859-4)
 162. Evangelidou N, Hamburger T, Cozic A, Balkanski Y, Stohl A (2017) Inverse modeling of the Chernobyl source term using atmospheric concentration and deposition measurements. *Atmos Chem Phys* 17(14):8805–8824. <https://doi.org/10.5194/acp-17-8805-2017>

Publisher's Note Springer Nature remains neutral with regard to jurisdictional claims in published maps and institutional affiliations.